1-30-2013

Nanomechanical characterization of asphalt

Hasan Faisal

Follow this and additional works at: https://digitalrepository.unm.edu/ce_etds

Student Name: Hasan Mohammad Faisal

Candidate

Graduate Unit (Department): Civil Engineering

Department

This thesis is approved, and it is acceptable in quality
and form for publication:

Approved by the Thesis Committee:

Rafiqul A. Tarefder, Chairperson

Yu-Lin Shen, Member

Walter Gerstle, Member

NANOMECHANICAL CHARACTERIZATION OF ASPHALT

BY

HASAN MOHAMMAD FAISAL

B.Sc. in Civil Engineering

Bangladesh University of Engineering & Technology, Dhaka, Bangladesh

THESIS

Submitted in Partial Fulfillment of the

Requirements for the Degree of

MASTER OF SCIENCE

Civil Engineering

The University of New Mexico

Albuquerque, New Mexico, USA

December 2012

DEDICATION

To my wife

ACKNOWLEDGEMENTS

NANOMECHANICAL CHARACTERIZATION OF ASPHALT

by

Hasan Mohammad Faisal

M.S. in Civil Engineering, University of New Mexico

Albuquerque, NM, USA 2012

B.Sc. in Civil Engineering, Bangladesh University of Engineering & Technology

Dhaka, Bangladesh 2007

ABSTRACT

In this study, asphalt binder and asphalt concrete (AC) materials are characterized using laboratory nanoindentation testing and mechanical models. Traditionally, laboratory nanoindentation test data is analyzed using the Oliver-Pharr method to determine elastic modulus and hardness of materials. In a nanoindentation test, a test sample surface is indented or loaded by a hard indenter tip and then unloaded. In the past, several studies of the polymer materials area have selected a loading rate and dwell time (i.e., the peak load is kept constant for a few seconds before unloading) to avoid or minimize the viscous effect of a material. No studies have attempted to examine the effects of dwell time and loading rate on viscous materials such as asphalt binder, which is the main topic of discussion in this study. This study focuses on determination of mechanical properties such as the elastic modulus and the hardness of viscoelastic materials, like asphalt, from nanoindentation load-displacement data. An existing spring-dashpot-rigid (SDR) element model developed by Oyen and Cook is employed as well as the well-established Oliver Pharr method. The SDR model uses the loading, holding and unloading time-

displacement data to predict the modulus, hardness and viscosity of the material. The model has shown excellent agreement with the laboratory indentation data of asphalt binder. Further, the SDR model is calibrated for nanoindentation test data of polymer modified asphalt binder. In addition, mechanical models such as the Voigt model and the Burger model are fitted to creep displacement and time data from nanoindentation tests to predict viscosity, retardation time and creep compliance for asphalt binder. All the models are found to fit very well with an average R^2-value of 0.99 for the Voigt model and R^2-value of 0.99 for the Burger model. Lastly, the nanoindentation test is performed on an AC (solid) sample to understand the aging in AC. Nanoindentation is done on two different parts of the AC sample: one on the mastic part (mix of asphalt binder and fines) and the other on the pure aggregate part. One hundred indentations were made in a single test on the mastic part to capture the heterogeneity. Approximately sixty indentations were made during a single indentation test on the aggregate part of AC. A small dwell time was applied to reduce the viscous effect of the mastic.

TABLE OF CONTENTS

LIST OF TABLES

LIST OF FIGURES

CHAPTER 1

INTRODUCTION

1.1 PROBLEM STATEMENT

Asphalt concrete (AC) is created by mixing asphalt binder with aggregate. Aggregate can be divided into two classes: coarse aggregate and fines. Coarse aggregate is defined by aggregate materials that are retained on a #200 sieve (75 micron). In hot mix asphalt (HMA), asphalt binder creates a coat or film around the coarse aggregates. Fines are defined as aggregate materials that pass through a #200 sieve. Fines are believed to be trapped inside an asphalt film creating a composite material called mastic. Therefore, AC has three major constituents: asphalt binder, mastic and coarse aggregate (Fig. 1.1). Mastic and asphalt binders play major roles in governing AC's behavior and performance. Over the years, test methods developed and performed to characterize mastic and asphalt binders have been limited to a few rheological tests. Moreover, the existing tests cannot be performed on mastic or asphalt binder film while they are integral parts of AC. Rather, those tests are performed on bulk liquid asphalt or mastic separately. Nanoindentation has created an opportunity to characterize mastic and asphalt binder while they are parts of AC.

Recently, a few researchers have performed macroscale and/or microscale tests on mastic such as the complex shear modulus test using a dynamic shear rheometer (DSR) or tension-compression test using a Dynamic Mechanical Analyzer (DMA) (You et al. 2010, Wang et al. 2011, Tarefder and Yousefi 2011). Almost all of the mastic tests were

performed on bulk mastic materials (i.e., solid and semisolid). Similarly, tests on bulk asphalt binders for measuring viscosity, shear modulus and stiffness properties in the laboratory are routine, whereas tests on the thin film of asphalt binder are not yet available in the asphalt industry. With the invention of nano- and micro- indentation techniques, it is now possible to indent aggregate, mastic and asphalt binder film while they reside in AC.

In general, the thickness of an asphalt binder varies from 10 to 15 microns, whereas the dimension of a mastic particle varies from 30 to100 microns. Though it may be possible to conduct microindentation testing (tip size varies from 30-45 micron) on aggregate and mastic, microindentation is not appropriate on asphalt binder for two reasons. Firstly, the size of a microindenter tip (average 30 microns) is larger than the thickness (average 10 microns) of an asphalt film. Secondly, the substrate effect is expected to be very high even if the asphalt film sample is prepared with a thickness of 80 microns. Though one can argue, microindentation has not been tried in this study, but it can be pursued in another study. Rather, nanoindentation tests were conducted on a thin film asphalt binder sample (thickness 80 microns) as well as on the aggregate and mastic phases of an AC sample. Nanoindentation was not tried on asphalt binder film or coatings in an AC sample because the available nanoindenter at the University of New Mexico (UNM) does not have a nanopositioner, which can precisely identify indentation locations.

In a nanoindentation test, an indenter is loaded to indent a sample surface and the movement or displacement of the indenter is measured as a function of the load. Load, displacement and time are recorded when the indenter indents and retracts. Usually, modulus of elasticity (E) and hardness (H) of a material are determined from load-

2

displacement data. Though the properties of hard materials such as metals and polymeric composites have recently been determined by nanoindenters, such properties of asphalt binder and mastic are unknown in the asphalt materials area. Elastic modulus and hardness of constituents of AC are rather attractive parameters for studying complex phenomena such as aging and/or moisture damage. Aging is believed to harden and stiffen an asphalt binder, whereas moisture damage is believed to weaken the mastic and binder phases. Due to the lack of a device or tests such as a nanoindenter to measure hardness and elasticity directly, asphalt researchers have so far characterized aged and unaged (bulk) asphalt binders using only shear modulus from a DSR test and bending stiffness from a Bending Beam Rheometer (BBR) test. An understanding of the phenomena of aging and/or moisture damage can be benefited or enhanced by measuring the elastic modulus and hardness of asphalt constituents using the nanoindentation technique, which is done here.

The nanoindentation test on asphalt binder film or mastic is non-trivial. Asphalt binder is a visco-elasto-plastic (VEP) material and a successful indentation test is affected by the viscous behavior of asphalt. To this day, the nanoindentation test is mostly performed on elastoplastic materials, which shows well-defined loading (elastoplastic) and unloading (elastic) behavior suitable for analyzing using the well-established Oliver-Pharr (1992) method. The Oliver-Pharr (1992) method of analysis uses the slope of the unloading (elastic) curve to determine modulus and hardness. In the case of VEP materials such as asphalt, the slope of the unloading curve becomes negative, as shown in Fig. 1.2, which cannot be used by the Oliver-Pharr method (1992). A few researchers have introduced a dwell time (when load is not increased) in an indentation test to avoid the negative slope

3

issue for determining properties from the unloading curve. Basically, viscous deformation is accomplished during dwell time and unloading becomes elastic (positive slope). Though dwell time (also known as creep loading time in traditional macroscale testing language) has been introduced in nanoindentation tests, the effects of dwell time and loading rate on the properties of VEP materials are largely unknown. To this end, this study determines the effect of dwell time and loading rate on the apparent elastic modulus and hardness properties of an asphalt binder in a nanoindentation test.

As is obvious from the previous discussion, loading and unloading data of a nanoindentation test on an elastoplastic material are analyzed to determine elastic modulus and hardness values. It is logical to analyze loading, dwell time and unloading data of a nanoindentation test on a VEP material (i.e. asphalt) to determine elastic (modulus), viscous (viscosity, retardation time) and plastic (hardness) properties. Like the Oliver-Pharr (1992) method, there is no straight forward solution or closed form equation to separate these behaviors. This study employs mechanical models such as the Burger model and the Voigt model to analyze nanoindentation creep data and determine viscoelastic properties of asphalt binder and mastic. In addition, an existing VEP model is modified to fit with nanoindentation data and determine elastic, viscous and plastic properties of an asphalt binder film. It can be noted that representing a material's behavior by mechanical models and properties is very useful for numerical modeling and/or a parametric study.

While this study is devoted to the nanoindentation of asphalt binder film, a limited number of nanoindentation tests are also conducted on aggregate and mastic phases of an AC sample. Test results are analyzed to compare the elastic modulus and hardness of

4

these two phases under aged and unaged conditions. In this study, nanoindentation tests are conducted only at room temperature (23±0.3 °C) because the temperature module for UNM's indentation device is not available.

1.2 OBJECTIVES

The main objectives of this study are to:

- Determine the effects of dwell time and loading rate on the apparent modulus of elasticity and hardness of an asphalt binder film using nanoindentation tests.

- Characterize elastic, viscous and plastic behavior of asphalt binders using existing/modified mechanical and VEP models to fit the nanoindentation test data.

- Compare elastic modulus and hardness of an aged and unaged mastic phase to those of an aggregate phase, both phases being integral parts of AC.

1.3 ORGANIZATION OF THE THESIS

Chapter 1 defines the problems associated with the nanoindentation of VEP materials such as asphalt. Review of recent nanoindentation studies of viscoelastic materials, theory of nanoindentation and mechanical modeling are presented in Chapter 2. In Chapter 3, the effects of loading and dwell time on the apparent modulus of elasticity and hardness of the asphalt binder are discussed. This chapter also includes asphalt material description, nanoindentation sample preparation and test data. In Chapter 4, existing mechanical models and a VEP model are modified and fitted to nanoindentation data by numerical optimization to separate viscous, elastic and plastic behavior of asphalt binder samples. In Chapter 5, elastic modulus and hardness of aggregate and mastic phases of an

AC sample are determined and compared. Finally, conclusions and recommendations based on this study are presented in Chapter 6.
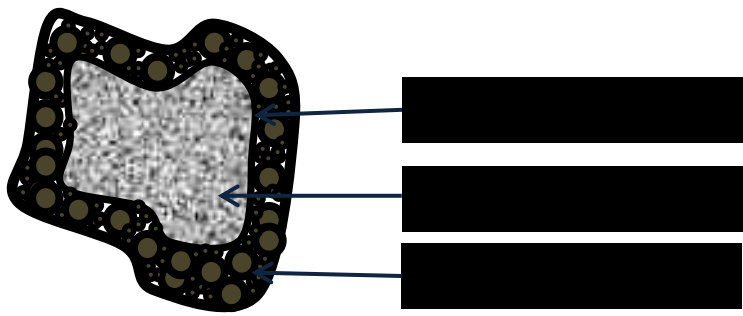
Figure 1.1 Asphalt Constituents in Asphalt Concrete (AC)
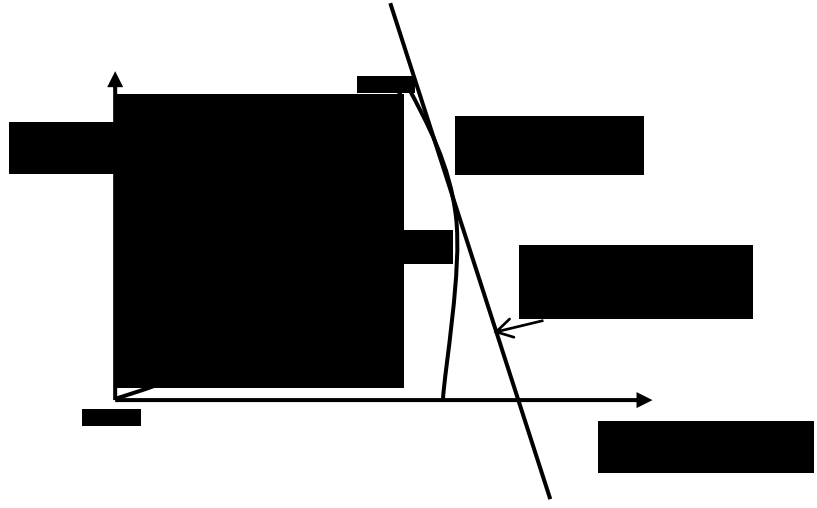
Figure 1.2 Negative unloading slope of load-displacement curve of nanoindentation test

CHAPTER 2

LITERATURE REVIEW

2.1 THEORY OF NANOINDENTATION

In a nanoindentation test, an indenter tip of a known modulus of elasticity and geometry is loaded to penetrate a sample surface and then unloaded. Modulus of elasticity of the sample is determined from the load-displacement data. The area of contact at full load is determined from the measured depth of penetration and the known geometry of the indenter tip. Sample hardness is calculated by dividing the maximum load by the contact area.

Several researchers have developed analytical methods to analyze load-displacement data to find elastic modulus and hardness. Doerner and Nix (1986) presented a method to calculate hardness from the loading curve and Young's modulus from the unloading curve. They assumed that the contact area remains constant as the indenter tip is retracted from the sample and the unloading curve is linear. Oliver-Pharr (1992) refined the Doerner and Nix method to account for the non-linear unloading curve, especially at the onset of unloading. According to the Oliver-Pharr method (1992), the vertical displacement of the contact periphery during the indentation test is modeled by the displacement of a ''flat elastic'' surface by a hard tip. The Oliver-Pharr method (1992) is the most widely used method to date for its simplicity.

A typical load displacement curve is shown in Fig. 2.1(a). A sitting load of 0.005 mN is typically applied initially to facilitate a contact between the tip and sample surface. Next, the load is increased gradually from point *a* to *b*. The tip is unloaded at the maximum

9

load point *b*. The unloading path is assumed to be elastic for most of the elastoplastic material. The unloading curve does not come back to point *a* due to plastic deformation in elastoplastic materials. The slope of the unloading curve at point *b* is usually equal to the slope of loading curve at point *a*.

Figure 2.1(b) shows the surface profile as a function of penetration depth during loading and unloading. Here, h_{max} is the total depth of indentation at a maximum load, h_p is the total depth of indentation that is unrecovered, h_s is the depth of the surface at the perimeter of the indenter contact and h_c is the vertical depth along which contact is made between the indenter and the sample. Therefore,

$$h_c = h_{max} - h_s \qquad (2.1)$$

The depth of impression that is recovered is,

$$h_e = h_{max} - h_p \qquad (2.2)$$

2.2 OLIVER-PHARR METHOD (1992)

The Oliver and Pharr (1992) method is based on the elastic contact between a rigid sphere (tip) and a flat surface (sample). Hertz (1986) found the contact radius *a* is related to the indenter radius *R*, applied load *P* and the reduced elastic modulus E^* of a sample by (see Fig. 2.2):

$$a^3 = \frac{3}{4}\frac{PR}{E^*} \qquad (2.3)$$

Contact radius *a* is also related to the indenter radius *R* and penetration depth by:

$$a = \sqrt{Rh} \qquad\qquad (2.4)$$

From Eq. (2.2) and (2.3) the applied load can be written as:

$$P = \frac{4}{3} E^* R^{1/2} h^{3/2} \qquad\qquad (2.5)$$

How to Find E*

If the indentation load P penetration depth h is recorded as the load displacement curve, the reduced elastic modulus E^* can be found from the load displacement curve as shown in Eq. (2.5). However, the equation also relates to the indentation radius. The equation can be simplified by differentiating Eq. (2.5) with respect to penetration depth h and using Eq. (2.4).

By differentiating Eq. (2.5) with respect to penetration depth h

$$\frac{dP}{dh} = \frac{4}{3} E^* R^{\frac{1}{2}} \left(\frac{3h^{\frac{1}{2}}}{2} \right) \qquad\qquad (2.6)$$

Using the relation in Eq. (2.4):

$$\frac{dP}{dh} = 2E^* \sqrt{Rh} = 2E^* a \qquad\qquad (2.7)$$

The projected area at the maximum load can be defined as: $A = \pi a^2$

Therefore,

11

$$S = \frac{dP}{dh} = \frac{2}{\sqrt{\pi}} E^* \sqrt{A} \tag{2.8}$$

where S is the unloading stiffness or slope of the unloading curve;

$$E^* = \frac{\sqrt{\pi}}{2\sqrt{A}} (S) \tag{2.9}$$

How to Find S

Oliver and Pharr (1992) used a power law function to fit the unloading path of the load-displacement curve. The power law function used by Oliver-Pharr is shown in Eq. (2.9):

$$P = \alpha(h - h_f)^m \tag{2.10}$$

where h is depth of penetration,

h_f is plastic depth,

α and m are curve fitting parameters related to tip geometry.

$m = 1$ for flat ended cylindrical tip, $m = 1.5$ for spherical tip, and $m = 2$ for conical tip (Berkovich tip).

Slope is measured by differentiation the in above Eq. (2.10) at onset of unloading.

How to Find A

Oliver and Pharr (1992) defined the projected area A as a function of h_c defined in Eq. (2.1). Oliver and Pharr (1992) extrapolated the tangent line to the unloading curve at the maximum loading point down to zero load. This yields an intercept value for depth which estimates the h_s by:

$$h_s = \varepsilon \frac{P_{max}}{S} \qquad (2.11)$$

Therefore,

$$h_c = h_{max} - \varepsilon \frac{P_{max}}{S} \qquad (2.12)$$

where ε is a geometric constant.

$\varepsilon = 0.72$ for conical tip, $\varepsilon = 0.75$ for Berkovich tip, and $\varepsilon = 0.72$ for spherical tip.

The project area is measured by:

$$A = \pi a^2 = \pi (Rh_c) \qquad (2.13)$$

where R is known and h_c is calculated using the above Eq. (2.9).

How to Find E

Timoshenko and Goodier (1951) found the reduced elastic modulus, E^* is related to the modulus of the indenter and the specimen and given by:

$$\frac{1}{E^*} = \frac{1 - \vartheta}{E} + \frac{1 - \vartheta_i}{E_i} \qquad (2.14)$$

where E is Young's modulus of the material,

ϑ is Poisson's ratio of the material,

E_i is Young's modulus of the indenter and

ϑ_i is Poisson's ratio of the indenter,

E^* is the reduced modulus. One can find the elastic modulus of the sample, E using Eq. (2.14).

How to Find Hardness, H

Hardness, H, is defined by the maximum load divided by the projected area (Brinell 1901):

$$H = \frac{P_{max}}{A} \tag{2.15}$$

where P_{max} = peak load and A = projected area of contact at the peak load. The unit of hardness is given in N/m^2=Pa.

2.3 INDENTER TIP SECTION

Tarefder et al. (2010) have used both spherical and Berkovich tips to indent asphalt binder. However, their study concluded that Berkovich tips are more suitable than spherical tips for asphalt testing. Spherical tips adhere to the asphalt sample surface. As a result, system compliance is lost during indentation on asphalt. Only Berkovich tips were used for asphalt testing in the current study.

For the Berkovich tip, the projected area of the contact is given by:

$$A = 3\sqrt{3}h_c^2 tan^2\psi \qquad\qquad (2.16)$$

where ψ= phase angle. The phase angle is ψ=65.27° for the Berkovich tip. Therefore, Eq. (2.17) can be simplified as:

$$A = 24.494\ h_c^2 \qquad or\ \ A \approx 24.5h_c^2 \qquad\qquad (2.17)$$

2.4 APPLICABILITY OF OLIVER-PHARR METHOD FOR VISCOELASTIC MATERIALS

As mentioned previously, the unloading portion of the load-displacement curve is fitted to the power law function according to the Oliver-Pharr method. The slope is determined by differentiating the load-displacement equation with respect to displacement. The unloading slope is positive for elastoplastic materials. Most of the cases the slope is negative for viscoelastic material. If slope is negative, the E^* becomes negative from Eq. (2.9). Therefore, this method is not applicable for viscoelastic material.

In viscoelastic materials such as asphalt, creep within the material can occur under indentation loading. Here "creep" means a time-dependent of deformation due to an applied load. Figure 2.3 shows schematically the load displacement curve of a viscoelastic material. It can be seen from the unloading portion of the load-displacement curve that displacement continues instead of recovery of displacement. The response is due to the viscous flow of the material. Therefore, the unloading portion of the load displacement curve becomes negative from Oliver-Pharr analysis method. Therefore, Oliver-Pharr method is not applicable.

2.5 PAST STUDIES OF NANOINDENTATION ON VISCOELASTIC MATERIALS

Li et al. (2001) studied the viscoelastic behavior of a polystyrene polymer using a nanoindenter and reported that the results are close to macroscale material properties.

Liu et al. (2006) used the Burger model to describe the behavior of polymeric materials subjected to nanoindentation. Their Burger model consisted of Maxwell and Kelvin elements. An analytical equation of the displacement of the indenter tip during loading and unloading was derived. Using the analytical solution they studied the elastic, viscous and plastic displacements during loading and unloading. They concluded that the Burger model is more suitable than the Maxwell model or the Kelvin model for studying viscoelastic behaviors of polymeric materials subjected to nanoindentation.

Jager et al. (2007) employed the nanoindentation technique to study the viscoelastic properties of asphalt. They conducted nanoindentation tests on two bitumen samples to understand the effect of loading rate, maximum load and temperature. They employed a non-linear dashpot and a power law creep model to describe the nanoindentation creep test results. It was shown that the maximum load has a significant effect on the model parameters, whereas the effect of loading rate is not very significant.

Yang et al. (2004) investigated the indentation creep behavior of polymers by using a flat-ended punch indenter and a Berkovich tip. These researchers proposed an elastic-visco-elasto-viscous (EVEV) model to describe the indentation creep behavior of polymers. According to this model, elastic modulus can be calculated by avoiding the use of the unloading data. As a result, their elastic modulus is independent of unloading rate.

16

Zhang et al. (2005) employed a five step nanoindentation loading to study the time independent mechanical properties of a viscoelastic material. They employed a Berkovich indenter with a maximum load of 8 mN applied for 2 sec and then immediately the load was reduced to 0.005 mN for 2 sec. After holding the load for 500 sec, creep load was applied for 2 sec and held for 2000 sec. For comparison, a conventional indentation creep test was also conducted (a step load of 8.000 mN was applied in 2 sec and then held for 2000 sec). They used a constitutive model to describe the elastic-viscoelastic behavior of polymeric materials and assumed the plastic deformation is negligible.

Wang et al. (2009) addressed the need for identification of mechanical properties of viscoelastic/plastic materials from nanoindentation data and developed numerical a finite element/optimization-based indentation modeling tool. A Creep test was carried out at a maximum load of 75 mN, using a 1 μm (nominal) radius conospherical tip.

2.6 LABORATORY AGING OF ASPHALT BINDER AND MASTIC

As asphalt is a multiphase material, it is logical to assume that each phase (say, mastic) is affected by an aging process differently. In this study, an asphalt concrete (AC) is subjected to oven aging (85 °C, 120±0.5 hours) and an aged sample is tested under nanoindentation. In particular, mastic and aggregate phases are indented and their hardness and elastic modulus are determined.
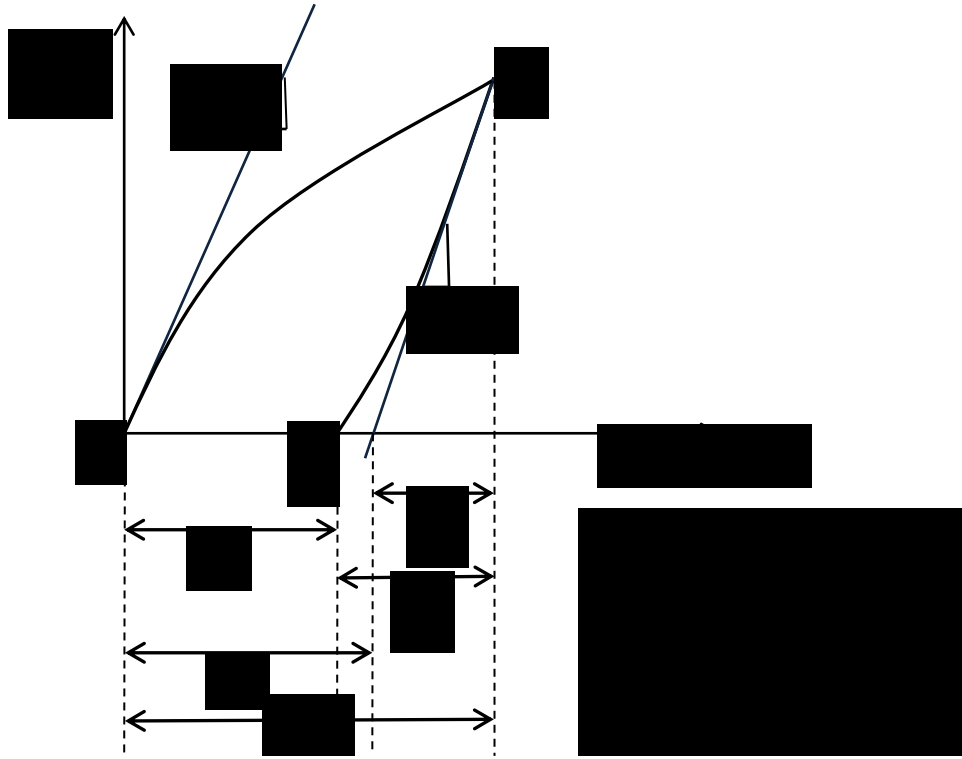
(a) Load −Displacement Curve
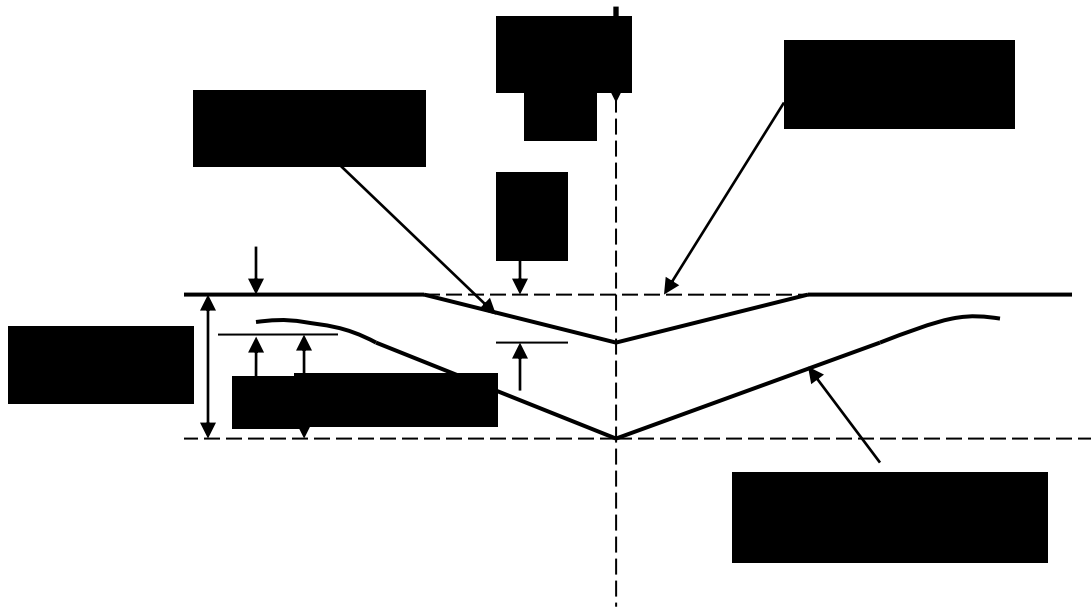
(b) Indentation Depth

Figure 2.1 Schematic of Indentation Test

18
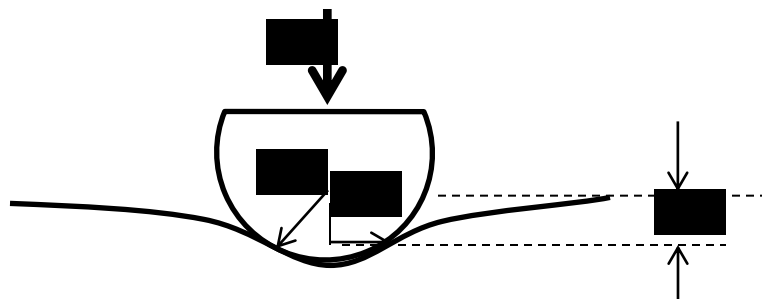
Figure 2.2 Indentation
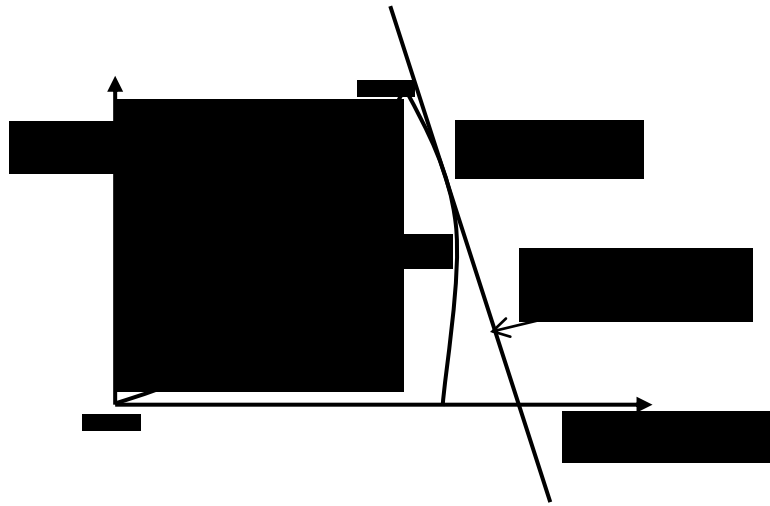
Figure 2.3 Nanoindentation and Viscoelasticity

CHAPTER 3

NANOMECHANICAL CHARACTERIZATION OF ASPHALT BINDER

3.1 INTRODUCTION

Nanoindentation is one of the most important techniques in recent days to measure

mechanical properties of materials at nano to micron depth from a sample's surface. In an

indentation test, a load P is applied on a flat sample and the resulting displacement h of

the small volume of material is recorded to determine the elastic modulus E and hardness

H of the sample (Doerner and Nix 1986, Oliver and Pharr 1992, Cheng and Cheng 1998).

The technique is predominantly used for mechanical characterization of hard materials

from their elastoplastic response (Wei et al. 2005, Zhang and Fang 2008). When the

technique is applied on soft material, the load-displacement P-h response leads to

indistinctness of mechanical characterization due to the viscous time-dependent behavior

of the material (Oyen and Cook 2002, Zhang et al. 2004, Lee et al. 2006). In recent years,

few researchers have attempted to characterize the viscoelastic behavior of soft polymer

using nanoindentation (Oyen and Cook 2002, Olesiak et al. 2009). The contact between a

nanoindenter tip and viscoelastic material exhibits simultaneously viscous flow and

elasticity behavior, not purely elastic behavior. This was clearly evidenced by the

extensive creep data obtained from indentation tests of polymer materials (Yang et al.

2004, Zhang et al. 2005, Wang and Ovaert 2008). The studies have shown that creep

occurs during unloading in a nanoindentation test of viscous materials. The use of the

unloading curve slope can lead to an overestimation of Young's modulus using the

Oliver-Pharr method. Other reserachers have shown that a "nose" appears in the

unloading load-displacement curve in cases of viscoelasticity (Briscoe et al. 1996, Briscoe et al. 1998). When the nose occurs, the stiffness or slope at the onset of unloading becomes negative, and the Young's modulus calculated by the Oliver-Pharr method, the most commonly used method for hard materials, is wrong.

There are a very few studies in the field for characterizing the viscoelastic properties of biological material and bones (Oyen et al. 2002, Bembey et al. 2006, Oyen and Ko 2007, Oyen et al. 2007, Olesiak et al. 2009). In particular, nanoindentation was used to determine mechanical properties of bones at the microstructural level (Tai et al. 2005). For viscoelastic materials, Oyen et al. (2007) developed a viscous-elastic-plastic (VEP) model for mechanical characterization of the material. According to the studies the model successfully predicts the viscoelastic material properties of bone material. Wu et al. (2011) studied the indentation creep behavior of bone with varying dwell or holding time. However, the introduction of the asphalt binder in the field of researchers of nanoindentation is rather limited (Ossa and Collop 2007, Ossa et al. 2005, Pichler et al. 2005). Asphalt binder is known to be a viscoelastic material that exhibits creep behavior. Tarefder et al. (2010) developed a range of indentation derived elastic modulus and hardness values of aged asphalt. Jager et al. (2010) studies the thermal effects on the mechanical properties of the asphalt binder. However, no research so far has attempted to examine the effects of dwell time and loading rate on nanoindentation behavior of asphalt binder.

One approach that has been suggested to obtain a more accurate elastic modulus of polymer materials is to allow sufficient time at peak load for the creep effects to minimize in an indentation experiment (Briscoe et al. 1998). Another approach is to

analyze indentation data recorded within a short dwell time before the unloading to remove the creep effects on both contact stiffness and contact area (Oyen et al. 2002). However, the apparent elastic modulus and hardness that leads to creep effects of material are dependent on dwell time, maximum load and loading/unloading rates for nanoindentation in polymer (Yang et al. 2004). Therefore, this study seeks to find an appropriate set of a loading rate and a dwell time for asphalt binder in a nanoindentation test that allows the test data to be analyzed for further characterization.

3.2 OBJECTIVES

The main objectives of the study are to:

- Examine the effects of dwell time and loading rate on apparent mechanical properties of asphalt binder in nanoindentation testing.
- Determine a loading rate and dwell time for asphalt binder that produces nanoindentation data that can be analyzed by the Oliver-Pharr method.

3.3 MATERIALS

In the study, the unmodified base asphalt binder was collected from Holy Asphalt Refinery, Albuquerque, NM. The Performance Grade (PG) of the binder is 58-28. The base binder was then modified using Styrene-Butadiene (SB) polymer. The SB polymer is mixed with base asphalt binder to make it resistant to flow (viscosity) and less affected by temperature change. The modifying binder was also collected from Holy Asphalt Refinery (Holy Asphalt, 2008).

3.4 MODIFYING ASPHALT BINDER WITH POLYMER

Three percent of SB polymer was used to modify asphalt binder. For modification of base binders were preheated up to 190°C in a one gallon container, with each of them containing 2 kg of asphalt binder. Then specified percent of polymer modifier added slowly to mix with a high shear mixer. Polymer was added slowly to ensure proper melting and mixing. Mixing of binders and polymers were done rapidly to minimize any effect of high temperature on binder properties. Adding polymer to the asphalt binder took around 20 minutes to 30 minutes. The modified binder was then put under the mixer for an extra 10min. Then the mix is cooled down to the room temperature.

3.5 AGING OF POLYMER MODIFIED ASPHALT BINDER

The asphalt binder aged using a standard test procedure for short term and long term aging. ASHTO T240 is used to simulate short term aging of asphalt binder using the RTFO test. In RTFO test the binder samples are aged at a temperature of 163°C for 85 minutes in rolling thin film oven under constant air flow. The residue of RTFO test is used for long term aging of binder. AASHTO R28 is used to simulate long term aging of asphalt binder in PAV. In PAV a constant temperature of 100°C and pressure of 2.1 atm is subjected on short term aged binder for 20 hours to simulate long term aging in it. To release all the air bubbles caused by the pressure a vacuum at 170°C is introduced for 30 minutes.

3.6 NANOINDENTATION

3.6.1 Sample Preparation

Polymer modified aged and unaged asphalt binder were used for testing so that they become resistant to flow and are less affected by temperature change. A polymer modified mixture of Styrene-Butadiene (SB) 3% asphalt binder was used for all the tests in the laboratory. Figure 3.1 shows a laboratory prepared asphalt binder film on glass substrate. As the first step, a glass slide surface 0.5 in × 0.5 in was selected and weighed in scale up to 4 significant decimal digits of grams. Next, the glass slide was wrapped with high temperature resistant tape. The tape was placed so that it formed the 0.25in^2 square gap area previously outlined for the binder. Then, hot polymer modified liquid asphalt binder was poured into the gap of the tape strips. The polymer-modified binders were melted by heating them to 163^oC for an hour. The asphalt coated surface was placed in the oven at 163^oC for 10 min in order to have a smooth surface, cooled at room temperature and the tapes were removed. Finally, the glass slide with the asphalt coating was weighed again to measure the amount of asphalt binder. From the known area, density of the asphalt binder and mass the thickness of the binder film was measured. The film thickness varied within a range of 40 μm to 80 μm.

3.6.2 Indentation Experiment

Indentation experiments were performed by using a nanoindenter manufactured in 2007 by MicroMaterials Ltd. Wrexham, UK. In all the tests the nanoindenter was equipped with the pyramidal Berkovich tip. The indentation tests were conducted in load control mode. In load control mode, the indentation includes a constant loading, unloading rate

and a holding segment at maximum load. A maximum load of 0.055 mN was applied with an initial load of 0.005 mN. The test matrix for loading, unloading rate and hold time is shown in Table 3.1. The selected dwell times were 70 sec, 100 sec, 150 sec and 200 sec for each set of loading and unloading rate. The loading, unloading rate and dwell times were selected so the tests could be performed in the thin film without hitting the glass substrate. The indentation depth remained small compared to the total material thickness so that the substrate effect on determining the mechanical property of the material could be avoided. The indenter moved at a rate of 1μm/sec to make the initial contact. In all the tests, the test camber temperature was kept at 26°C, within a fluctuation of ±0.2°C. After the test, the temperature corrections were also provided to the analysis. In the test, for each set of test setup, 5 indentations were made on the sample with a distance of 300μm, which is shown in Fig. 2. The distance was selected to avoid the pile up and sink in effect for successive indentations. However, according to ASTM guidelines, the required distance needed to be at least six indent radii away from the previous indentation point. Because of the soft bulk of the asphalt binder, the pile up effect could be more. Furthermore, there was no limitation of space in the sample in nanoscale. For these reasons, a substantial distance was chosen for testing the material. 70 indentations were conducted in the asphalt binder samples and 5 indentations for each set of loading, unloading rate and dwell time.

3.7 RESULTS & DISCUSSION

3.7.1 Unaged Binder

Several attempts were made to indent several unaged asphalt binder samples. However, the indentation on unaged asphalt binder was found to be very challenging. In many

cases, the indentation failed to detect contact surface, which is a major requirement of nanoindentation testing. Typically, a nanoindentation tip approaches the sample's surface and penetrates. During penetration, if the tip is resisted by some force, which is the case with a hard sample, the tip stops, thus the surface of the thin film material is introduced for nanoindentation. However, in a sample of unaged asphalt binder, the resistance force was too low. As a result, the tip continued to penetrate and failed to detect the contact surface of the unaged asphalt.

Although the tip could not detect the contact surface on unaged asphalt binder, trials were made. In general, after the contact surface was developed, the tip was retracted to a retardation distance of 100-200 μm before the penetration test on the sample. During the trials on unaged asphalt binder, a few of the binder samples were able to contact the surface. This prepared the nanoindentation tip for the indentation test. The tip was retracted for a specified retardation distance, as shown in Fig. 3.2. The figure shows the retracting tip moving away from the sample with a buildup of asphalt binder substance on its tip. The attached binder can be seen as a continuous thread from the binder film to the nanoindentation tip. Because of this, the machine was unable to make further indentations on the sample, making trials impossible. Figure 3.3 shows the retracting tip, as it moves up to a retardation distance of 400 μm. The resulting thread connection between the film and binder became thinner and separated. However, some of the binder material mass remained on the nanoindentation tip, therefore it can no longer carry out the test as a nano tip. The impression on the asphalt binder film, as shown in Fig. 3.4, made it impossible to indent on the same position where the tip first detected the surface. The figure shows the pileup of soft asphalt on the film.

Based on these trials, it can be concluded that unaged binder cannot be analyzed through well-known analysis methods under nanoindenter conditions due to its low stiffness and viscous behavior. However, a new test can be developed to infer the material property analyzing the thread thickness and thread length for specific loading condition. An unaged frozen sample might be possible to test, although it was not tried in this study.

3.7.2 Aged Binder

Based on the trials on unaged binder, several nanoindentation tests were done on the polymer modified aged binder. The aging was done in rolling thin film oven for simulating the short term aging in the binder and followed by pressure aged vessel for simulating the long term aging in the binder. The test on the aged binder was successful because of its less viscous property. In this case, the nanoindenter was able to detect the contact surface and the machine was able to sense the displacement of the binder with increasing load. As a consequence of the ramp load, i.e., load, dwell time and unload, the binder showed load displacement curves like those in Figure 3.5. The figure shows five load displacement curves for a specific loading and unloading rate of 0.002 mN/sec and dwell time of 100 sec. The five curves correspond to five indentation points in the asphalt binder.

Load displacement behavior of aged binder at short dwell time

Several nanoindentation attempts were made on the aged asphalt binder sample, beginning with a dwell time of 20 sec. However, the dwell time of 20 sec was too short a time to overcome the viscous effect of the asphalt binder. Further, the 20 sec dwell time intervals and two separate loading rates were introduced to the binder to determine

28

whether the increased loading rate worked for the binder. The decision was made by working with the unloading curve of the load displacement curve. If the unloading curve of the binder showed no nose effect, the load displacement curve could be introduced to the Oliver-Pharr analysis for further discussion. Figure 3.6(a) shows the load displacement curve with 20 sec dwell time and loading and unloading rates of 0.002 mN/sec for 5 indentations. However, because of the predominant creep behavior of the binder, a negative slope in the unloading portion of the load-displacement curve is found. To ensure the predominant creep effect, another five indentations were conducted again with dwell time of 20 sec and an increased loading, unloading rate of 0.005 mN/sec as shown in Fig. 3.6(b). For this case, the unloading curve shows the same nose effect on the unloading portion of the load displacement curve.

Effect of dwell time on unloading portion of the load displacement curve

Figure 3.7 shows the effect of dwell time at maximum load on the unloading portion of the load displacement curve. The figure shows load displacement curve of 5 nanoindentations on aged asphalt material. For all the indentations the loading, unloading rates remained constant at 0.002mN/sec. The figure shows the maximum nose effect for the load displacement curve of dwell time of 20 sec. As the dwell time increases from 20 sec to 200 sec the viscous effect of the material decreases. The lowest viscous effect was found in lowest value at a dwell time 200 sec. The study shows that with a dwell time greater than 50 sec the material starts to decrease in the bowing out or nose effect of the unloading portion of the curve. Hence, the viscous effect of the material decreases with increase in the creep load on the thin film binder. Decrease in the nose effect of the unloading portion of the load displacement curve leads the slope curve to shift from

negative to positive. This makes the curve possible to analyze by the Oliver-Pharr method. However, since an increase in the dwell time or creep load time in the binder shows an increase in the positive slope value of the material, asphalt binder needed to be further analyzed to reduce the uncertainty in the nanomechanical property of the material.

Statistical analysis to determine the effect of loading, unloading rate and dwell time on nanoindentation test results

As an increase in the dwell time gives the asphalt binder a positively sloped load displacement curve, it is possible to analyze the load displacement curve of the binder through Oliver-Pharr method. In the study, the Oliver-Pharr method is employed to determine the apparent reduced elastic modulus and the hardness of the material and to see whether the loading, unloading rate and dwell time effect the results. To find the significance of influence of the loading, unloading rate and dwell time in the asphalt binder film, all the test matrix results were exercised for two factors ANOVA analysis with replication. The statistical information was introduced with α value of 0.05, and the result of P value for dwell time and loading, unloading rate was less than the α value. Therefore, it can be concluded that the effect of loading, unloading rate and dwell time for the indentation test is significant. Table 3.2 shows the results of ANOVA analysis on the obtained results of the tests. Since, the tests loading and unloading rates are constant, they are used as a single variable for the analysis. The P value for apparent reduced elastic modulus is much less than the hardness value of the material.

Trend of hardness and reduced elastic modulus of asphalt binder with increase in the dwell time at maximum load

Investigation on the apparent hardness of the asphalt binder shows that it is a function of dwell time. As the dwell time increases, the apparent hardness of the material decreases to a fixed value. However, all the values of hardness converge to a fixed value after 200 sec of dwell time, as shown in Fig. 3.8. Here the plot is done for average value of 5 indentation tests with the same loading, unloading rate and dwell time at maximum load. Therefore, it can be concluded that a dwell time of greater than 200 sec would reduce the viscous effect of the asphalt binder to a minimum level. Apparent hardness and reduced modulus of the material also found to be a function of dwell time. Figure 3.9 shows a decrease in the trend for apparent reduced modulus for increase in dwell time.

Combined effect of dwell time and loading rate in normalized modulus and hardness value

Figure 3.10 shows the normalized relationship between apparent hardness of the material and dwell time and loading rate. It can be noticed here that at first with small dwell time the higher loading, unloading rate starts with higher hardness value and when the dwell time is increased its becomes almost the same as lower loading, unloading rates for the material. However, as the dwell time increases to 200 sec the apparent hardness of the material tends to be a lower value and close to zero. From Fig. 3.11 it is noticeable a normalized relationship of apparent modulus of the material with dwell time for different loading and unloading rates. Though the graph shows an increase in pattern for modulus/hardness for increasing dwell time, it may be because the apparent hardness of

the material decreases more rapidly than the modulus, which makes the resultant increasing.

3.8 CONCLUSIONS

- In the study, combined effects of loading rate and dwell time are studied on unaged and long-term aged asphalt binder, which is a time-dependent viscoelastic material. The indentation response of the unaged binder was found to be challenging due to its very high viscous effect of the material at service temperature. For the indentation load rates and dwell time considered, the apparent material property was found to be a function of both the variables.

- The unloading portion of the load-displacement curve strongly depends on the dwell time for the long-term aged asphalt binder. 200 sec of dwell time, the binder converges to a fixed value for all loading and unloading rates employed in the material. For testing of asphalt binder, a dwell time of 200 sec is recommended for further study. Load-displacement curves are analyzed by Oliver-Pharr analysis and the binder shows a decreasing value of apparent hardness and apparent reduced elastic modulus with increasing dwell time.

- Investigation of loading rates on the binder, found that at low dwell time, effect of was significant and at high dwell time the apparent material properties tend to merge in a constant value. However, at low dwell time, i.e., less than 50 sec, the unloading portion of the load-displacement curve showed a bowing out effect, irrespective of loading/unloading rates.
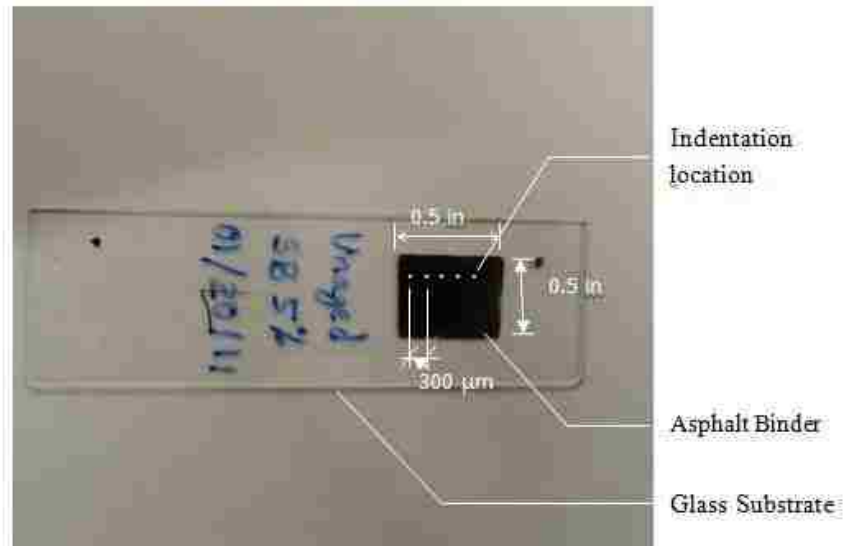
Fig. 3.1 Asphalt Binder Sample for Nanoindentation
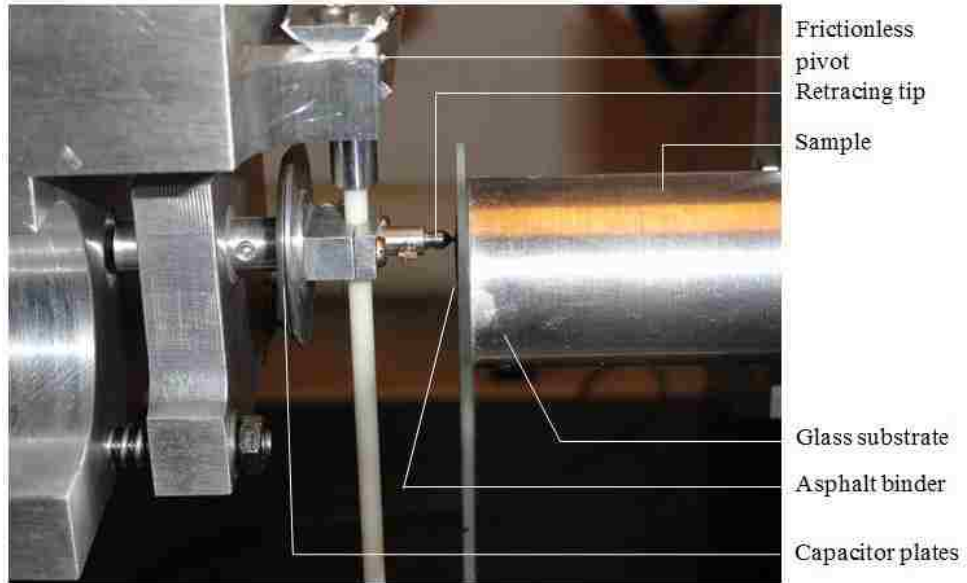
Fig. 3.2 Nanoindentation on Unaged Sample
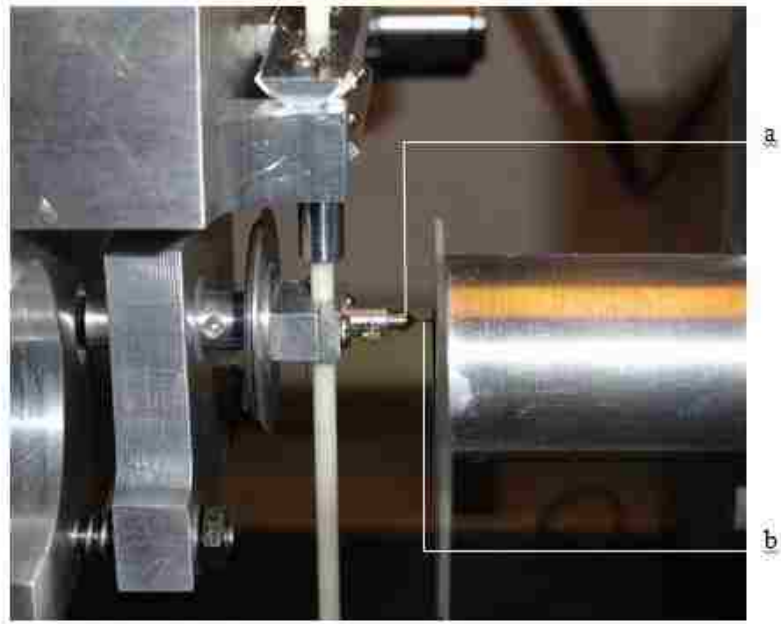
Fig. 3.3 Retardation Distance of Nanoindentation Tip from the Sample on Unaged Binder: (a) Retracing Nanoindenter Tip; (b) Thread of Unaged Asphalt Binder to Retardation Distance of 400 µm

Piled up asphalt

Asphalt binder

Glass substrate Sample
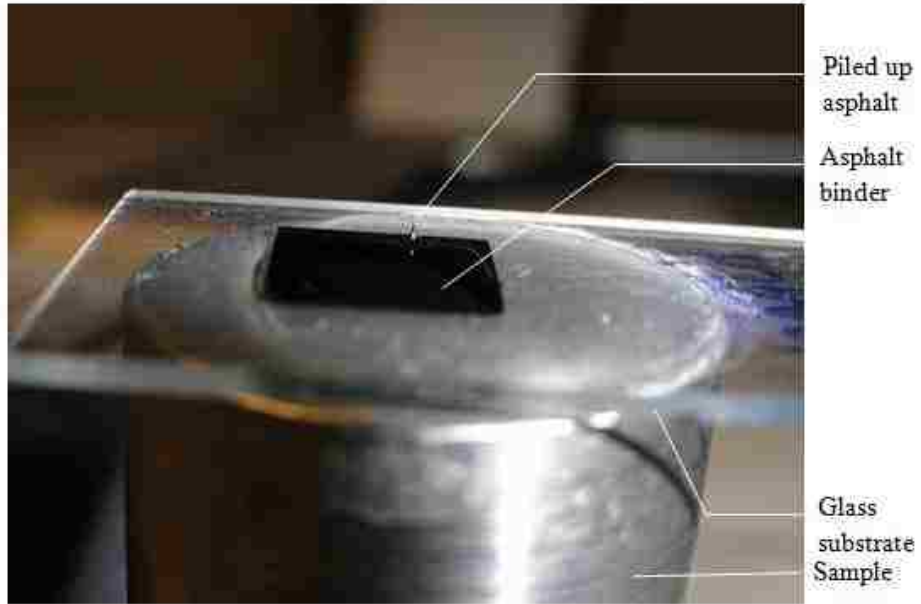
Fig. 3.4 Impression of Indentation Tip on Unaged Binder
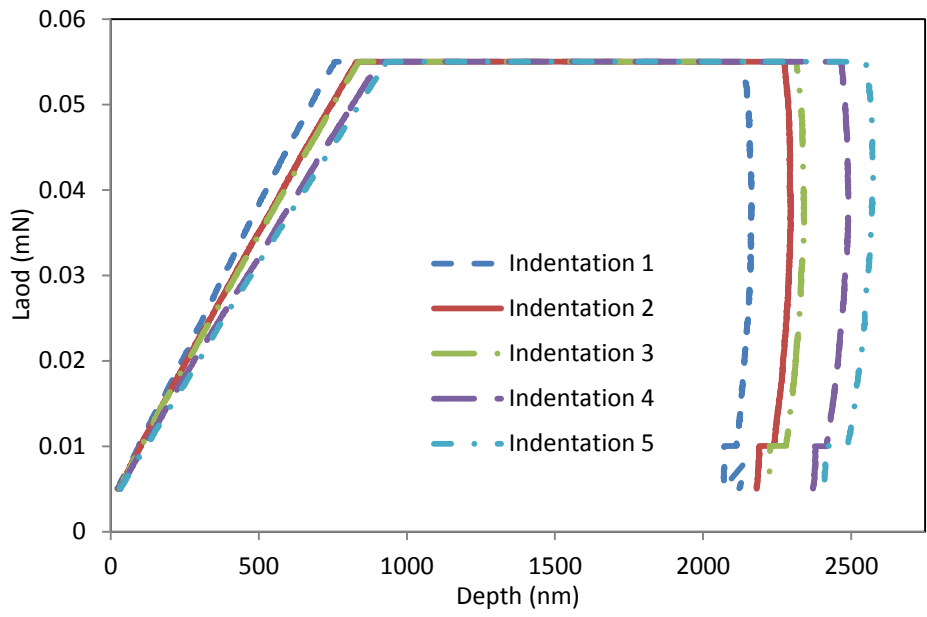
Figure 3.5 Nanoindentation Load Displacement Curve
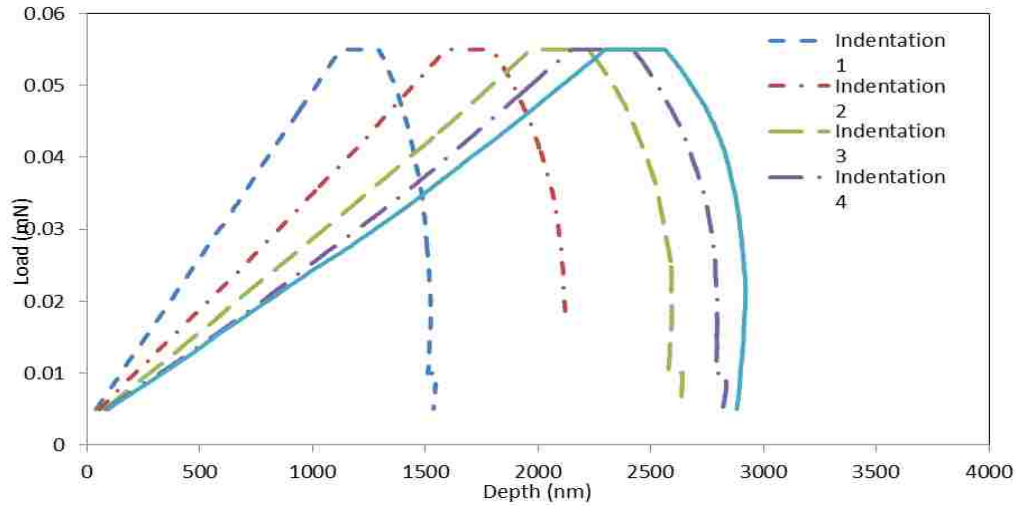
(a)
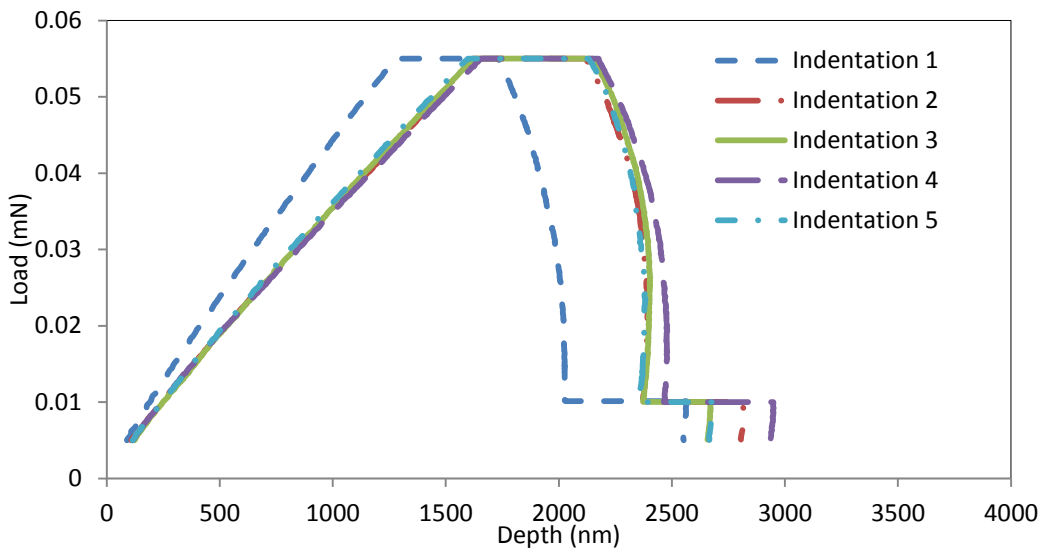
(b)

Figure 3.6 Nanoindentation Test for Small Dwell Time: (a) Nanoindentation Load Displacement Curve Loading Rate 0.002 mN/sec, Dwell Time 20 sec ; (b) Nanoindentation Load Displacement Curve Loading Rate 0.005 mN/sec, Dwell Time 20 sec
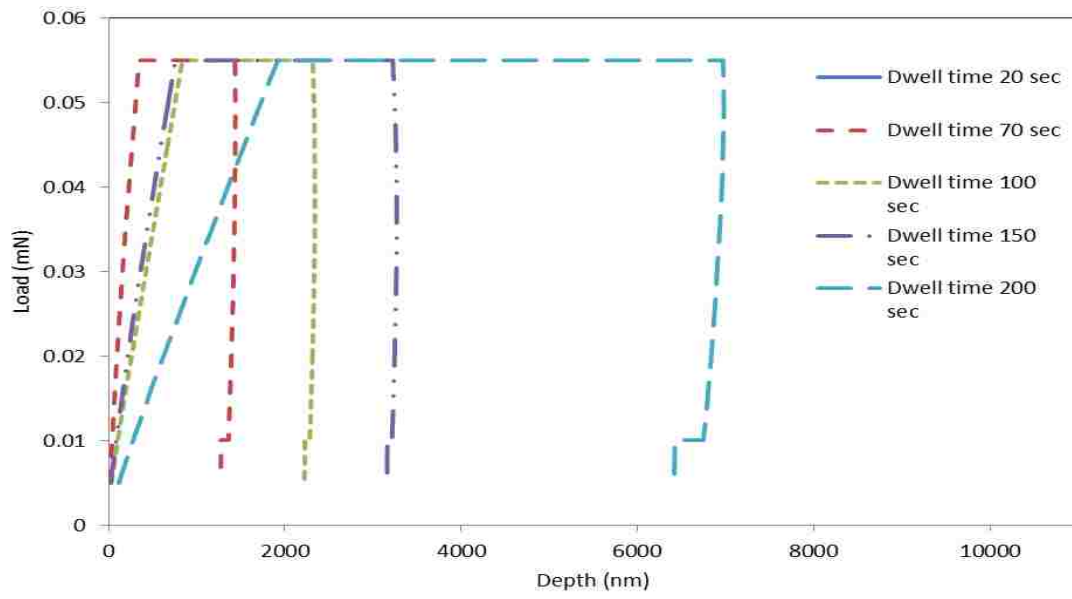
Figure 3.7 Effect of Dwell Time on the Unloading Curve
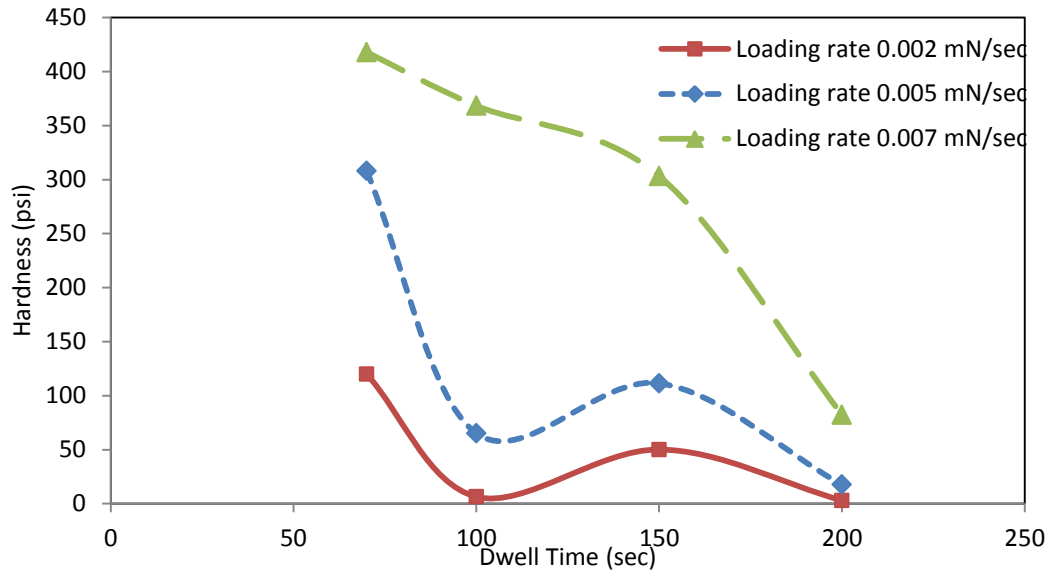
Figure 3.8 Effect of Increase in the Dwell Time on Apparent Hardness of the Material
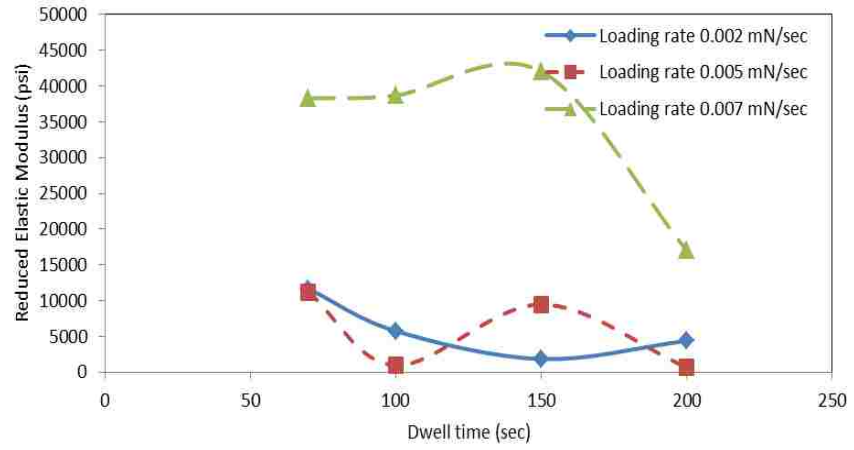
Figure 3.9 Effect of Increase in Dwell Time on Apparent Reduced Elastic Modulus of the Material

41
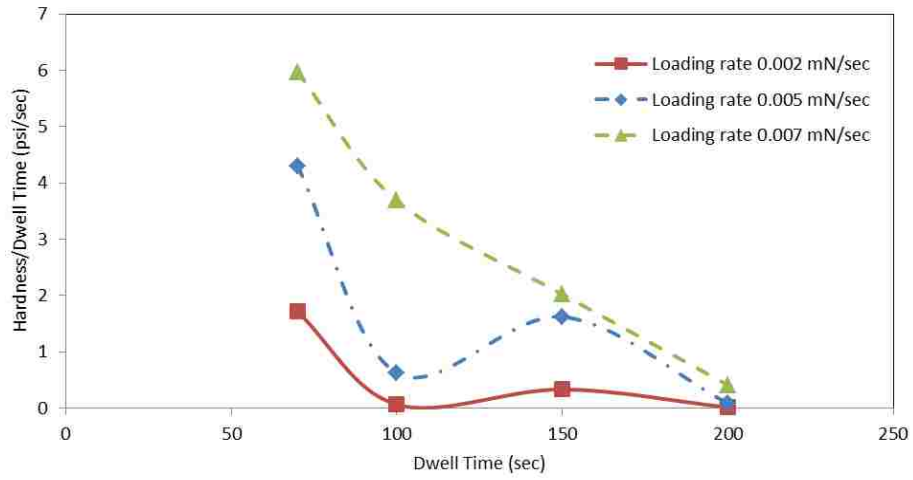
Figure 3.10 Normalized (Hardness/ Dwell Time) vs. Dwell Time for Different Loading
Rate
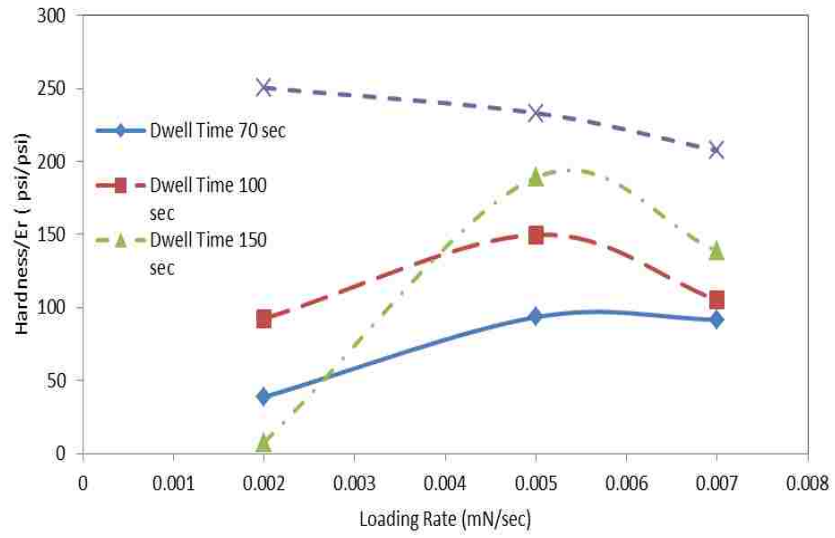
Figure 3.11 Normalized (Er/Hardness) vs. Loading Rate for Different Dwell Time

Table 3.1 Test Matrix for Nanoindentation Test on Asphalt Binder

Dwell Time (sec)	Loading / Unloading Rate (mN/sec)		
	0.002	0.005	0.007
70	×	×	×
100	×	×	×
150	×	×	×
200	×	×	×

Table 3.2 ANOVA Analysis Result for Both Hardness and Reduced Modulus of the Data

P value for	Hardness	Reduced Elastic Modulus
Effect of Loading rate	2.09E-10	3.41E-29
Effect of Dwell time	3.11E-08	3.4E-11
Prescribed α value for the analysis is 0.05.		

Note: Loading & unloading rate were constant in every test

CHAPTER 4

MODELING NANOINDENTATION CREEP BEHAVIOR OF ASPHALT BINDER

4.1 INTRODUCTION

Nanoindentation has recently been used to understand time dependent creep behavior of viscoelastic materials such as asphalt (Oyen and Cook 2003; Yang et al. 2004). As discussed previously, in a nanoindentation test, an indenter is loaded to indent a sample surface and the movement or displacement of the indenter is measured as a function of load. Load, displacement, and time are recorded during the test. Elastic modulus (E) and hardness (H) of the sample are determined from load-displacement data. To this day, nanoindentation test is mostly performed on elasto-plastic materials, which show well-defined loading (elasto-plastic) and unloading (elastic) behavior suitable for analyzing using well established Oliver-Pharr method (1992). Oliver Pharr method of analysis uses the slope of the unloading (elastic) curve in modulus calculation (Oliver and Pharr 1992). In case of visco-elasto-plastic materials such as asphalt, the slope of the unloading curve becomes negative due to continuous viscous flow. The material is essentially unloaded visco-elastically, instead of elastically. Therefore use of such unloading data in Oliver-Pharr method results in inaccurate value of modulus of elasticity (Oyen and Cook 2003; Zhang et al. 2004; Lee et al. 2006). A few researchers have introduced a dwell time during which load is not increased, to avoid any viscous flow during unloading (Briscoe et al. 1996; Briscoe et al. 1998, Feng 2002). Though introduction of a dwell time reduces the viscous effect on elastic modulus, exactly what dwell time is appropriate for asphalt is

not known. If the dwell time is short, viscosity may affect the unloading curve, which may lead to an underestimation of modulus. Therefore, it is logical to analyze load-displacement data during dwell time (or creep) of a nanoindentation test on viscoelastoplastic materials. To this end, the Burger and the Voigt models are used to determine the modulus of elasticity (spring) and viscosity (dashpot) from creep data. Also, the entire load-displacement curve, which includes loading, creep, and unloading, is fitted to a rheological model that includes spring, dashpot, and rigid elements. This model is called SDR model and used to separate elastic, viscous, and plastic properties of asphalt binders.

The viscous behavior of asphalt is traditionally defined by parameters such as viscosity, creep compliance, and retardation time. These parameters are usually obtained from macroscale laboratory testing. For example, a macroscale viscometer test is used to measure viscosity of asphalt binder in the laboratory. Similarly, a bending beam rheometer test is used to determine creep compliance. A Dynamic shear rheometer test is used for determining retardation time and so on. If viscosity, compliance and retardation time can be obtained from a single nanoindentation test, the test method would be very useful for asphalt materials design and to the asphalt industry. In the past, a few researchers in polymer materials area have fitted indentation data to different rheological models and constitutive models to determine viscoelasticity (Wang and Ovaert 2008, Monclus and Jennett 2011, Huang and Lu 2006,Yang et al. 2004, Wu et al. 2011, Isaksson et al. 2010, Zhang et al. 2005, Oyen and Cook 2007, Olesiak et al. 2010). However, such a study to fit mechanical models to nanoindentation creep data has not been performed in the asphalt area. Only limited success in determining the hardness and

modulus of asphalt has been reported (Tarefder et al. 2010, Jager et al. 2006). Therefore, the current study has employed rheological models to analyze nanoindentation data in determining the viscous and elastic properties of asphalt binder for the first time.

4.2 OBJECTIVES

The primary objectives of this study are to:

• Determine viscosity and retardation time by analyzing nanoindentation creep data with mechanical models such as the Voigt model, the Burger model and elastoviscoplastic or SDR model.

• Determine elastic modulus of an asphalt binder during nanoindentation tests.

4.3 METHODOLOGY

Sixty nanoindentation tests were conducted at four dwell time and three loading rates, as described in chapter 3. Laboratory test data were presented in chapter 3 and therefore, they are not reported in this chapter.

4.4 VISCOELASTIC SOLUTION OF BERKOVICH INDENTER

The load-displacement response of an indenter is expressed by a quadratic elastic load-displacement relationship, shown in Eq. (4.1) (Oliver and Pharr 1992, Oyen and Cook 2003).

$$P_0 = \frac{\pi \tan \psi}{2\gamma^2} \frac{E'}{(1 - \nu^2)} h^2 \qquad (4.1)$$

where P_0 = indentation load

h = displacement due to applied load in a material

E = elastic modulus of indented material

v = Poisson's ratio of the material

ψ = include half angle of Berkovich indenter (i.e. 70.3°) and

γ = constant relates contact depth to total depth and is taken as unity for polymeric materials. For asphalt materials, $\gamma = 1.0$ was assumed.

The Eq. (4.1) can be rearranged as:

$$h^2 = \frac{2}{\pi}\frac{P_0 \, cot\psi}{E} \tag{4.2}$$

where E is the plain strain modulus.

$$E = \frac{E'}{1 - v^2} \tag{4.3}$$

The elastic expression in Eq. (4.2) can be modified to develop a viscoelastic expression, by replacing P_0/E, with an integral over a creep function $J(t)$, known as creep compliance, as shown below:

$$h^2 = \frac{2cot(\psi)}{\pi}\int_0^t J(t-u)\frac{dP_0(u)}{du}du \tag{4.4}$$

where $J(t) = 1/E$, is creep compliance and u, is a dummy variable for integration and delayed response is presented by *(t-u)* variable instead of time variable *t*.

4.5 VOIGT MODEL

Figure 4.1 shows the Voigt model considered for this study. It has a linear spring and a dashpot element in parallel with a linear spring in series. The linear spring follows Hooke's law, which states that stress is proportional to the strain.

$$\sigma = E\epsilon \tag{4.5}$$

where σ is stress, ϵ is strain and E is the elastic modulus of the spring.

The dashpot represents the behavior of a viscous material. It states that stress is proportional to the time rate of strain.

$$\sigma = \eta \frac{\partial \epsilon}{\partial t} \tag{4.6}$$

where η is viscosity and t is time.

Under constant stress Eq. (4.6) can be integrated to become:

$$\epsilon = \frac{\sigma t}{\eta} \tag{4.7}$$

The dashpot and the spring parallel to it will have the equal displacement response. Both the spring and the dashpot have the same strain, but the total stress is the sum of two stresses, using the subscript from Fig. 4.1,

$$\sigma = E_2\epsilon_2 + \eta_2\frac{\partial\epsilon_2}{\partial t} \tag{4.8}$$

where E_2 is elastic modulus of parallel spring and η_2 is viscosity of parallel dashpot. If a constant strain is applied:

$$\int_0^\epsilon \frac{d\epsilon_2}{\sigma - E_2\epsilon_2} = \int_0^t \frac{dt}{\eta_2} \tag{4.9}$$

or

$$\epsilon = \frac{\sigma}{E_2}[1 - \exp(-\frac{t}{\tau_2})] \tag{4.10}$$

where τ_2 is retardation time.

$$\tau_2 = \frac{\eta}{E_2} \tag{4.11}$$

The additional series spring element of Voigt model has an instantaneous elastic strain. Therefore, the total strain,

$$\epsilon = \frac{\sigma}{E_1} + \frac{\sigma}{E_2}[1 - \exp(-\frac{t}{\tau_2})] \tag{4.12}$$

where E_1 is the elastic modulus of the series spring.

It can be seen from Eq. (4.12) that

when $t = 0$ and if $E_1 = E_2 = E$, then the instantaneous strain $\epsilon_1 = \sigma/E$;

51

when $t = \infty$ and if $E_1 = E_2$, $\epsilon_2 = 2\sigma/E$, or the spring is fully stretched to its total retarded strain;

when $t = \tau_2$ and if $E_1 = E_2$, $\epsilon_3 = (2 - 1/e)\sigma/E$. Now, $\epsilon_3/\epsilon_2 = (2 - 1/e)/2 = 70.5\%$ or $\epsilon_3 = 70.5\%$ of ϵ_2.

Thus, the retardation time τ_2 of Voigt model is the time to reach 70.5% of the total retardation strain.

Eq. (4.12) can be rearranged as:

$$\frac{\epsilon}{\sigma} = \frac{1}{E_1} + \frac{1}{E_2}[1 - \exp(-\frac{t}{\tau_2})] \tag{4.13}$$

Therefore, the basic creep compliance equation for Voigt model is,

$$J(t) = \frac{1}{E_1} + \frac{1}{E_2}\left[1 - e^{-t/\tau_2}\right] \tag{4.14}$$

4.5.1 Determination of Voigt Model Parameter

For a constant load P_0 in the Voigt model, replacing $J(t)$ values of Eq. (4.4), one can find:

$$h^2 = \frac{2}{\pi}P_o \cot \psi \left[\frac{1}{E_1} + \frac{1}{E_2}\left(1 - e^{-\frac{t}{\tau_2}}\right)\right] \tag{4.15}$$

For known values of $(h, P_0$ and $t)$ from an indentation test, the values of E_1, E_2 and τ_2 can be obtained from Eq. (4.15).

Load displacement data during dwell time are used to find Voigt model parameters (spring E and dashpot τ). Data (h,t) during load increase and unloading data not used.

Specifically, Eq. (4.7) is fitted to indentation creep data. Eq. (4.7) can simply be expressed in the following form:

$$h^2 = A_1 + A_2\left(1 - e^{-t/\tau_2}\right) \tag{4.16}$$

Where $A_1 = \frac{2}{\pi} P_o \cot \psi \, (1 - v^2)\frac{1}{E_1}$ and $A_2 = \frac{2}{\pi} P_o \cot \psi \, (1 - v^2)\frac{1}{E_2}$.

The constants A_1 and A_2 are found by fitting indentation data to Eq. (4.16) using nonlinear optimization. The creep constants and the spring constants are obtained by further solving A_1 and A_2. Nonlinear least square algorithm was scripted in Matlab to minimize the sum of squared error between the experimental data and the predicted data. Figure 4.2 compares Voigt model predicted data to five laboratory indentation data.

4.5.2 Results and Discussion

Eq. (4.16) is fitted to sixty test data by least square optimization and model parameters are shown in Table 4.1. Retardation time from Voigt model varies from 43 sec to 331 sec with an average value of 111 sec. The spring constants E_1 is found to be 71.46 Pa and E_2 is found to be 9 Pa. The retardation time τ_2 increases as the dwell time increases, as shown in Table 4.1. From Table 4.1 it can also be seen that retardation time increases as the loading rate increases. Figure 4.3 shows the creep compliance obtained from Voigt model. Figure 4.3 (a) shows creep compliance for dwell time 200 sec and Fig. 4.3 (b) shows creep compliance for dwell time 150 sec. A decrease in loading rate shows higher creep compliance for both dwell times.

4.6 BURGER MODEL

Figure 4.4 shows a Burger model which has a dashpot in series with Voigt elements.

The strain of the dashpot from Eq. (4.7) can be expressed as:

$$\epsilon_{Dashpot} = \frac{\sigma t}{\eta} \qquad (4.17)$$

Adding Eq. (417) with Eq. (4.12) gives the viscoelastic solution for Burger model:

$$\epsilon = \epsilon_{Dashpot} + \epsilon_{Voigt}$$

$$(4.18)$$

$$\epsilon = \frac{\sigma t}{\eta_1} + \frac{\sigma}{E_1} + \frac{\sigma}{E_2}[1 - \exp(-\frac{t}{\tau_2})]$$

The equation can be rearranged as:

$$\frac{\epsilon}{\sigma} = \frac{1}{E_1} + \frac{1}{E_2}\left[1 - \exp\left(-\frac{t}{\tau_2}\right)\right] + \frac{t}{\eta_1} \qquad (4.19)$$

Therefore, the basic creep compliance equation for Burger model is,

$$J(t) = \frac{1}{E_1} + \frac{1}{E_2}[1 - e^{-t/\tau_2}] + \frac{t}{\eta_1} \qquad (4.20)$$

4.6.1 Determination of Burger Model Parameter

For a constant load P_0 in the Burger model, replacing $J(t)$ values of Eq. (4.4), one can find:

$$h^2 = \frac{2}{\pi} P_o \cot \psi \left[\frac{1}{E_1} + \frac{1}{E_2}\left(1 - e^{-\frac{t}{\tau_2}}\right) + \frac{E_1 t}{\tau_1}\right] \qquad (4.21)$$

For known value of (h, P_0, t) from an indentation test, the values of E_1, E_2, τ_1 and τ_2 can be obtain from Eq. (4.21).

$$h^2(t) = A_1 + A_2\left(1 - e^{-t/\tau_2}\right) + A_3 t \qquad (4.22)$$

where $A_1 = \frac{2}{\pi} P_o \cot \psi \, (1 - \vartheta^2) \frac{1}{E_1}$, $A_2 = \frac{2}{\pi} P_o \cot \psi \, (1 - \vartheta^2) \frac{1}{E_2}$ and $A_3 = \frac{2}{\pi} P_o \cot \psi \frac{E_1 t}{\tau_2}$

Eq. (4.22) is fitted to laboratory data to find A_1, A_2 and A_3.

4.6.2 Results and Discussions

The Burger model captured the indentation creep. Burger model shows the similar trend of retardation time as the Voigt model as given in Table 4.2. The value of spring constant E_1 is found to be 80 Pa and E_2 is found to be 50 Pa from optimization of Burger model. Retardation times are determined from specific loading rate and dwell time. Table 4.2 shows an decrease in retardation time with the increase in the dwell time. However, retardation time for parallel dashpot element decreases with the increase in loading rate.

4.7 SPRING-DASHPOT-RIGID (SDR) MODEL WITH NONLINEAR SPRING

With the SDR model, the behavior of asphalt material under nanoindentation creep is modeled by three quadratic elements as shown in Fig. 4.5 (Oyen and Cook 2003; Olesiak et al. 2010). The model is called Spring-Dashpot-Rigid (SDR) element model. Load-displacement relations of spring, dashpot and rigid elements are nonlinear, more specifically quadratic. Load-displacement relation of spring is defined as:

$$P_e = k_Q h_e^2 \qquad (4.23)$$

where k_Q is the quadratic stiffness. The quadratic stiffness is identified with the plain strain modulus of the material, E', via geometric considerations: $k_Q = \alpha_1 E'$ and $\alpha_1 = \pi/(2cot\psi)$. The second element is defined by a dashpot as follows:

$$P_v = \mu_Q \left(\frac{dh_v}{dt}\right)^2 \qquad (4.24)$$

where μ_Q is a quadratic viscous coefficient. The quadratic viscosity is the product of geometric term α_2 and a material property: $\mu_Q = \alpha_2 \eta$. Here η is the indentation viscosity and geometric term $\alpha_1 = \alpha_2$. Under indentation conditions, substantial plastic deformation can occur beneath the indenter. The third element is defined by a rigid body as follows:

$$P_P = \alpha_3 H h_p^2 \qquad (4.25)$$

where P_P and h_p are the load and displacement on the rigid body element. H is the plastic deformation resistance or hardness of the material, and $\alpha_3 = \pi tan^2\psi$ is a dimensionless geometry parameter for sharp indentation with effective included angle 2ψ. The dimensionless constants are for Berkovich tip as: $\alpha_3 = \pi tan^2\psi = 24.5$ and $\alpha_1 = \alpha_2 = 4.4$ (Oyen and Cook 2003).

The total displacement is the result of sum of displacements in three elements, can be written as:

$$h = h_v + h_e + h_p \tag{4.26}$$

where h is the total displacement, h_e is the elastic displacement in spring, h_v is the viscous displacement in the dashpot and h_p is the plastic displacement in the rigid element.

Load in the elements can be written as:

$$P = P_e = P_v = P_P \tag{4.27}$$

As the displacement is the sum of displacement for three individual elements, the displacement rate is also the sum of the displacement rates of the individual element, which gives the following equation:

$$\frac{dh}{dt} = \frac{dh_v}{dt} + \frac{dh_e}{dt} + \frac{dh_p}{dt} \tag{4.28}$$

Substituting the values of Eq. (4.12), Eq. (4.13) and Eq. (4.14) in Eq. (4.17):

$$\frac{dh}{dt} = \frac{P^{1/2}}{(\alpha_2\eta)^{1/2}} + \frac{1}{P^{1/2}}\frac{dP}{dt}\frac{1}{2(\alpha_1 E')^{1/2}} + \frac{1}{P^{1/2}}\frac{dP}{dt}\frac{1}{2(\alpha_3 H)^{1/2}} \tag{4.29}$$

Nanoindentation Load

A trapezoidal indentation load, as shown in Fig. 4.6 was considered. The loading and unloading rates were kept constant. The creep hold or dwell time was applied at the maximum load. Here, k represents the loading and unloading rate, t_R represents loading and unloading time, and t_c represents the dwell time.

Loading Curve

The slope of the loading curve can be expressed as:

$$P(t) = kt \tag{4.30}$$

$$\frac{dP}{dt} = \frac{dP_e}{dt} = \frac{dP_v}{dt} = \frac{dP_P}{dt} = k; \quad 0 \le t \le t_R \tag{4.31}$$

Substituting the slope value in Eq. (4.29):

$$\frac{dh}{dt} = \frac{(kt)^{1/2}}{(\alpha_2 \eta)^{1/2}} + \frac{1}{(kt)^{1/2}} \frac{k}{2(\alpha_1 E')^{1/2}} + \frac{1}{(kt)^{1/2}} \frac{k}{2(\alpha_3 H)^{1/2}} \tag{4.32}$$

By integrating Eq. (4.32):

$$h^{LOAD}(t) = (kt)^{1/2} \left(\frac{2t}{3(\alpha_2 \eta)^{1/2}} + \frac{1}{(\alpha_1 E')^{1/2}} + \frac{1}{(\alpha_3 H)^{1/2}} \right) \tag{4.33}$$

Creep Curve

Slope during holding time can be expressed as:

$$\frac{dP}{dt} = 0; \quad t_R \le t \le t_C + t_R \tag{4.34}$$

Substituting this in Eq. (4.29) and integrating the resulting equation gives:

$$h^{CREEP}(t) = \int_{t_R}^{t_C + t_R} \frac{(P_{max})^{\frac{1}{2}}}{(\alpha_2 \eta)^{1/2}} dt \tag{4.35}$$

$$h^{CREEP}(t) = \frac{(P_{max})^{\frac{1}{2}}}{(\alpha_2 \eta)^{1/2}} (t - t_R) + h^{LOAD}(t_R) \tag{4.36}$$

Unloading Curve

Slope of unloading curve can be expressed as:

$$\frac{dP}{dt} = -k; \quad t_R + t_C \leq t \leq 2t_R + t_C \qquad (4.37)$$

Thus the unloading rate can be defined as:

$$\frac{dh}{dt} = \frac{[k(2t_R + t_C - t)]^{1/2}}{(\alpha_2 \eta)^{1/2}} - \frac{1}{[k(2t_R + t_C - t)]^{\frac{1}{2}}} \frac{k}{2(\alpha_1 E')^{1/2}} \qquad (4.38)$$

The solution for unloading portion is given by (Olesiak et al. 2010):

$$h^{UNLOAD}(t) = (k)^{\frac{1}{2}} \left(\frac{t_R^{\frac{3}{2}} - (2t_R + t_C - t)^{\frac{3}{2}}}{\frac{3}{2(\alpha_2 \eta)^{1/2}}} \right.$$

$$\left. + \frac{(2t_R + t_C - t)^{\frac{1}{2}} - t_R^{\frac{1}{2}}}{(\alpha_1 E')^{1/2}} \right) + h^{CREEP}(t_R + t_C) \qquad (4.39)$$

Eqs. (4.33), (4.36) and (4.39) defines the entire displacement-time history of a nanoindentation test of asphalt using trapezoidal loading.

4.7.1 Determination of SDR Model Parameters

Nanoindentation data is used to fit the above Eqs. (4.33), (4.36) and (4.39). Displacement data is fitted first to Eq. (4.36) to estimate viscosity η. Next, the unloading data is fitted to Eq. (4.39), to estimate all the model parameters. Table 4.3 shows the model parameters, that can be obtained from loading, creep and unloading curve. The curve

fitting of the displacement time curve was done in Matlab using nonlinear least square fitting, with using trust region algorithm.

4.7.2 Results and Discussions

Table 4.4 shows the average of obtained data from the SDR model. Average value of apparent modulus is obtained from five indentation tests for a specific dwell time. Model parameters obtained from whole load displacement response of nanoindentation. The SDR model successfully captured the viscoelastic response of the material, as shown in Fig. 4.7. In Fig. 4.7 the predicted model parameters are used to validate an experimental load-displacement curve. The predicted modulus of the material decreases an increase in dwell time. As the dwell time of the nanoindentation test increases the indenter indentation depth increases and the depth increase affects the modulus prediction from the model. The hardness value also follows the similar trend of modulus. However, its rate of change decrease of hardness value with increase in dwell time is higher than that of elastic modulus, as the plastic deformation resistance of the material decreases with increase in indentation depth. The decrease of viscosity with increase of dwell time is analogues with the previous study of nanoindentation on viscoelastic material, which states the introduction of increased dwell time decreases the viscous effect of the material (Feng and Ngan 2002). Therefore, the apparent viscosity of the material decreases with increase in dwell time. The previous study on the polymeric and biological material also shows the same trend (Zofka and Nener-Plante 2011).

Comparison between Oliver-Pharr Method and Nonlinear SDR Model

It is a common practice to eliminate the viscous effect through an extended creep hold time for viscoelastic material (Briscoe et al.1998, Feng and Ngan 2002). Therefor the applied extended dwell time on asphalt thin film made the indentation load displacement data to be analyzed by Oliver-Pharr analysis. Since, the extended dwell time makes the unloading curve portion of the indentation load displacement curve positively sloped. Table 4.5 shows the result comparison between the SDR model and traditional Oliver-Pharr method. The result comparison shows Oliver-Pharr method assessing the modulus and hardness value with much lower range as the method is not considering the time dependent response of the material, whereas SDR model estimates the modulus and hardness value in higher range. However, the hardness value estimation is close to the hardness values in Oliver Pharr analysis.

The lower estimation of modulus and hardness value from Oliver-Pharr analysis could be resulted from the existing viscous effect in the binder, though extended creep hold is introduced in the indentation experiments. The extended creep hold may not eliminate all of viscous effect on the asphalt binder. Therefore, full elastic analysis of indentation load displacement curve as in Oliver-Pharr analysis, can resulted in error to extract the material physical properties. However, the validation in nano scale needs some other analysis, like molecular dynamics simulation.

4.8 SDR MODEL WITH LINEAR SPRING

The fitting of SDR model showed some discrepancy in fitting the loading portion of the load displacement curve. Therefore, the model is further modified with linear spring response instead of quadratic response of the spring element (Fig. 4.7).

The linear spring response modifies the basic spring equation of indentation in Eq. (4.23).

$$P_e = k_Q h_e \qquad (4.40)$$

The linear spring response also changes the viscous-elastic-plastic response equation for loading and unloading. However, the equation of holding does not change, as it includes only the viscous response of the material. The equations for loading, creep and unloading are:

Loading Curve

$$h^{LOAD}(t) = (kt)^{1/2} \left(\frac{2t}{3\left(\alpha_3 \eta_Q\right)^{1/2}} + \frac{(kt)^{1/2}}{E'} + \frac{1}{(\alpha_1 H)^{1/2}} \right) \qquad (4.41)$$

Creep Curve

$$h^{CREEP}(t) = \frac{(P_{max})^{\frac{1}{2}}}{(\alpha_2 \eta)^{1/2}} (t - t_R) + h^{LOAD}(t_R) \qquad (4.42)$$

Unloading Curve

$$h^{UNLOAD}(t) = (k)^{\frac{1}{2}} \left(\frac{t_R^{\frac{3}{2}} - (2t_R + t_C - t)^{\frac{3}{2}}}{2\left(\alpha_3 \eta_Q\right)^{1/2}} + \frac{(k)^{\frac{1}{2}}(2t_R + t_C - t)}{E'} \right)$$
$$+ h^{CREEP}(t_R + t_C) \qquad (4.43)$$

Parameter determination of the calibrated equations are done in similar approach as in previously employed for quadratic spring response equation. However, the LSDR model

fitting decreased the R^2 value due to the linear curve in loading and unloading load displacement curve. The model was not able to predict the curvature of the unloading curve as well as of the loading curve.

E and H from Oliver-Pharr vs. SDR Model

Table 4.6 shows the averaged value of modulus and hardness as a function of dwell time. Here the values of modulus, hardness are extracted from the LSDR model. The model parameter shows similar trend that found in the previous SDR model. The predicted modulus value decreases with increase in dwell time. Similar declining trend found in for hardness of the material as well.

In comparison between Oliver Pharr method, SDR model and LSDR model Table 4.6 shows that both model prediction of modulus and hardness is close to each other. However, there are some anomaly between two model predictions of hardness and elastic modulus for dwell time of 150 sec and 200 sec. For linear spring response model the hardness values are close the Oliver Pharr prediction as well.

4.9 APPLICATION NOTE

This study has clearly shown how nanoindentation data can be modeled to separate elasticity, viscosity and hardness of an asphalt binder. The results are particularly useful for characterization the viscoelastic behavior of thin film asphalt binder. Viscosity, creep compliance and retardation time of asphalt binder are very useful parameters for defining flow behavior of asphalt binder. The modulus value and hardness value of asphalt binder can be used to characterize aging, healing and moisture damage in asphalt. Creep

compliance and retardation time are used to model low temperature cracking and shear induced permanent deformation.

4.10 CONCLUSIONS

Nanoindentation data is modeled using Voigt, Burger and SDR model. The following conclusions can be made:

- Voigt model is defined by a spring and a dashpot in parallel with additional spring in series. Modulus of spring in series is found to be 9.0 Pa and spring in parallel is around 72 Pa. Apparent retardation time of parallel dashpot varies with loading rate and dwell time. Apparent retardation time decreases with the increase in loading rate and dwell time. However, for a specific loading rate and dwell time the retardation time is constant, e.g. for loading rate 0.002 mN/sec and dwell time of 70 sec the retardation time is around 57 sec.

- In the study, Burger model is defined by an extra dashpot element with Voigt model elements. For Burger model, modulus of spring in series is found to be 80 Pa and spring in parallel is around 51 Pa. Apparent retardation times of series and parallel dashpot varies with loading rate and dwell time. Apparent retardation time in parallel increases with the increase in loading rate and dwell time. However, apparent retardation time in series decreases with the increase in loading rate and dwell time.

- In the study, SDR model is used to predict the load displacement behavior of asphalt binder for sharp nanoindentation. The simulation of the indentation behavior extracts the material properties, e.g. viscosity, modulus and hardness. The model successfully simulates the experimental load displacement behavior.

- The SDR model outputs are compared with the traditional Oliver-Pharr method. Because of the application high creep time at constant load the load displacement curves are able to analyze through traditional Oliver-Pharr analysis. The SDR model outputs are found larger than that of Oliver Pharr method. Though the validation of the output results need some other study, like molecular dynamics simulation.

- SDR model predicts viscosity of the material in addition to prediction of modulus and hardness. The model output follows the same trend like in mechanical models, i.e. viscosity of the material decreases with increase in dwell time. The model predicted modulus and hardness values are higher than Oliver Pharr method.

- Nonlinear SDR model is further calibrated with linear spring response so that it can predict exact load displacement behavior of asphalt thin film. However, the calibration found to be predicting the load displacement behavior with lower R^2 value. The calibrated LSDR model predicted modulus, hardness values found close to the quadratic spring response model prediction. Thus, original SDR model with quadratic spring response element is recommended for prediction of viscoelastic material property.
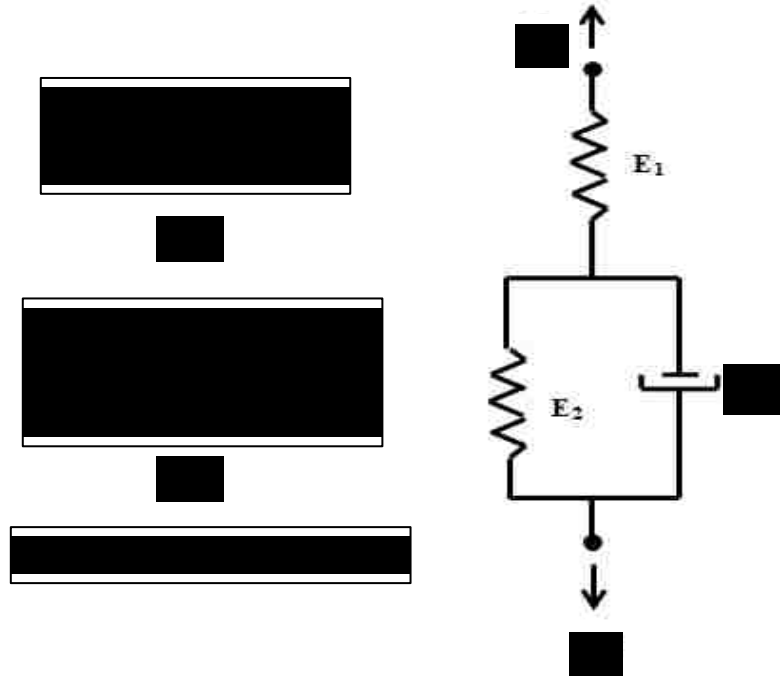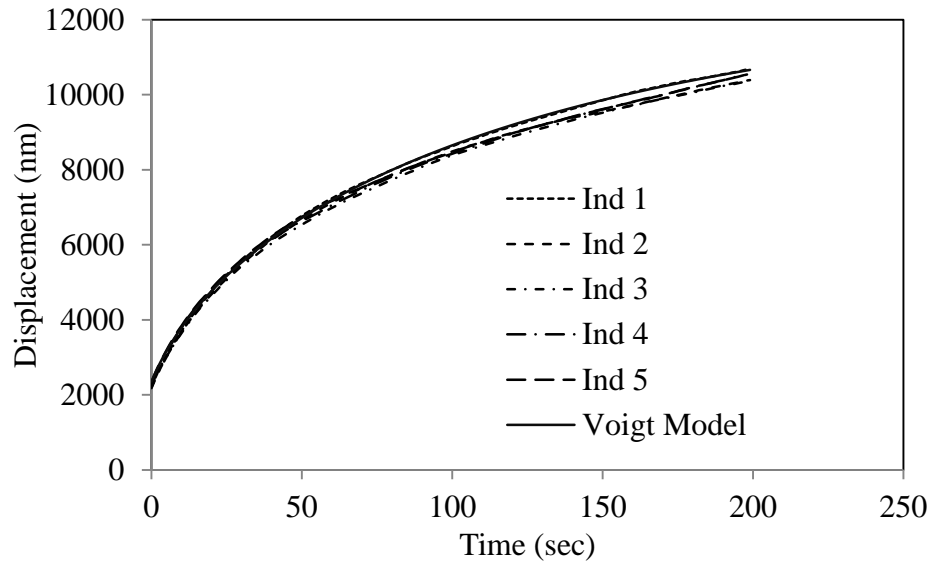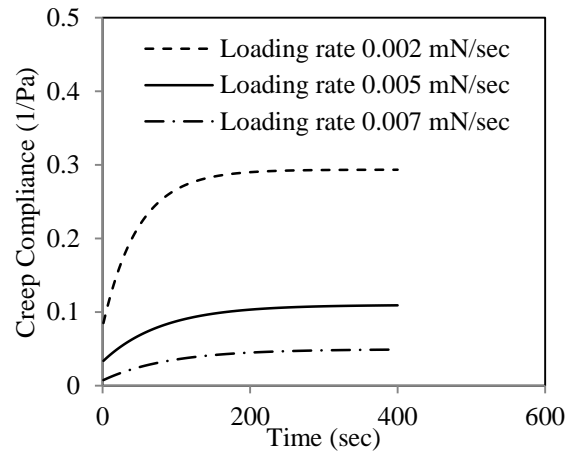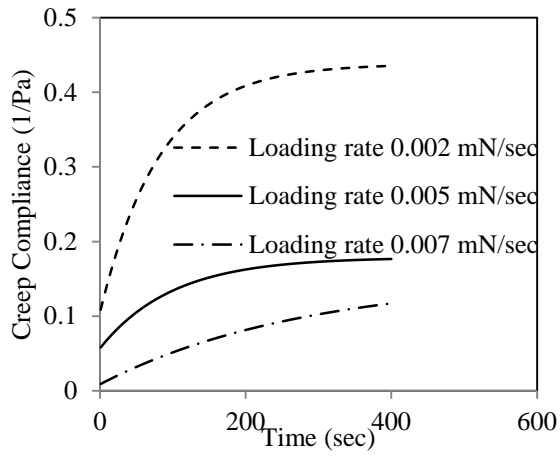
Figure 4.1 Voigt Model

Figure 4.2 Voigt Model Fitting

(a) Represents dwell time of 200 sec   (b) Represents dwell time of 150 sec

Figure 4.3 Creep Compliance from Voigt Model
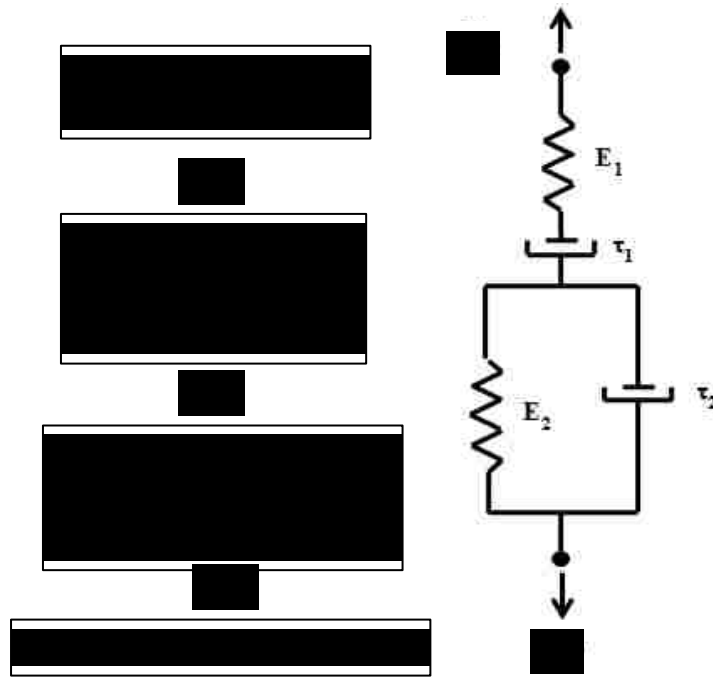
Figure 4.4 Burger Model

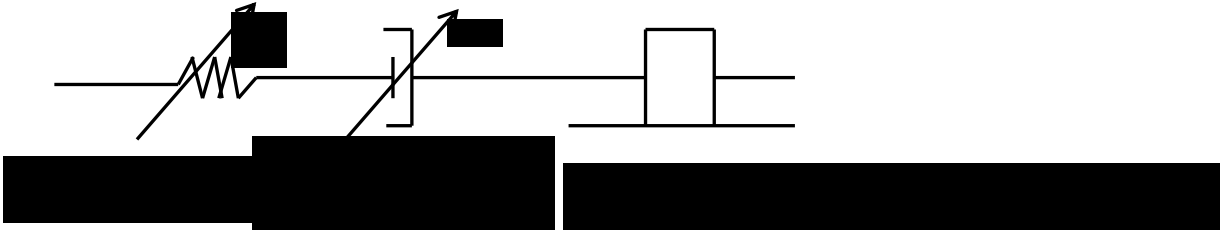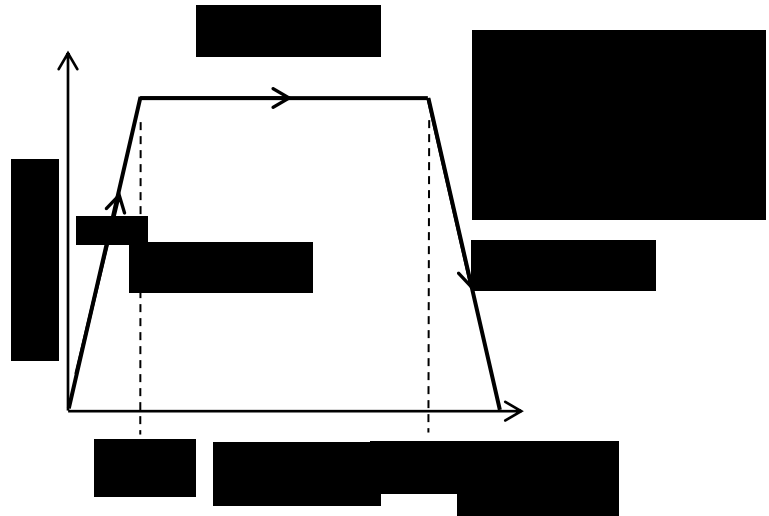**Figure 4.5** Spring-Dashpot-Rigid Element Model

Figure 4.6 Indentation Load
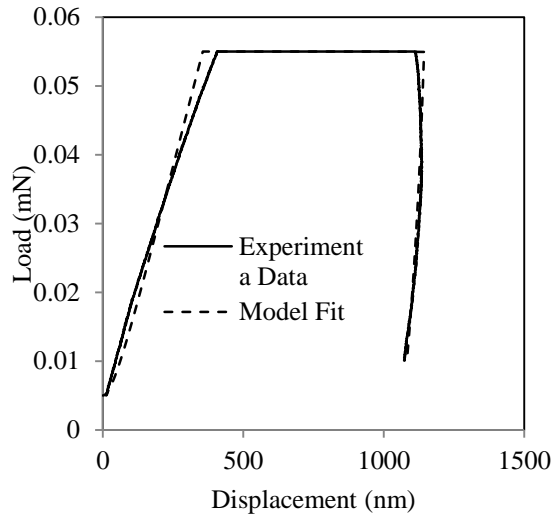
(a) Represents the Validation of Load Displacement Curve for Dwell of 70 sec
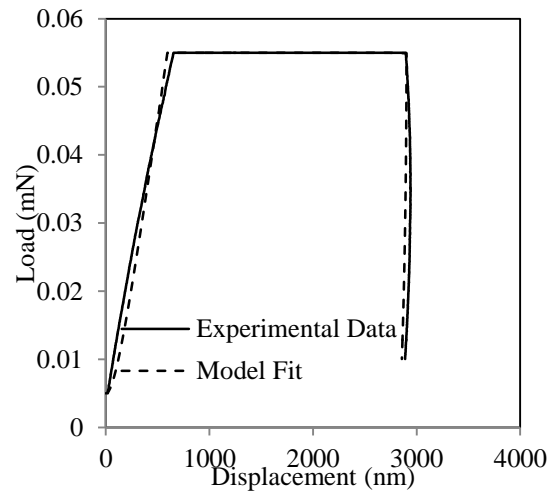
(b) Represents the Validation of Load-Displacement Curve for Dwell Time of 200 sec

Fig. 4.7 Load Displacement Curve Prediction of SDR Model and Experimental Data
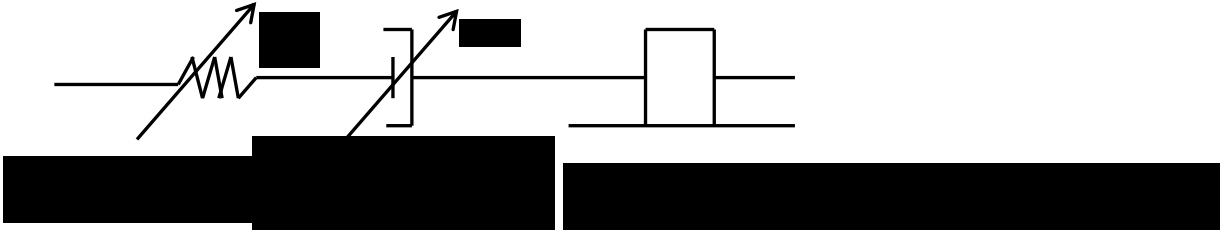
Figure 4.8 Calibrated Oyen Cook Model for Linear Spring Response

Table 4.1 Elastic Modulus and Retardation Time for Voigt Model

Parameter	P_0 (mN)	E_1 (Pa)	E_2 (Pa)
All loading Rates & Dwell Times	0.055	72.46	9

Dwell Time	Retardation Time, τ_2 (sec)		
	Loading Rate (mN/sec)		
	0.002	0.005	0.007
70 sec	56.9±3.1	94.1±11.2	63.7±3.1
100 sec	48.3±1.9	80.3±5.7	89.7±6.8
150 sec	82.3±3.4	99.4±8.9	121.5±9.4
200 sec	136.2±7.0	181.6±17.5	280.8±30.4

Table 4.2 Elastic Modulus and Retardation Time for Burger Model

Parameter	P_0 (mN)	E_1(Pa)	E_2(Pa)
All loading Rates & Dwell Times	0.055	80	50.9

Dwell Time	Retardation Time, τ_1 (sec)			Retardation Time, τ_2 (sec)		
	Loading Rate (mN/sec)			Loading Rate (mN/sec)		
	0.002	0.005	0.007	0.002	0.005	0.007
70 sec	0.0036 ±0.00025	0.0023 ±0.00038	0.0014 ±0.00011	30.8±6.4	23.4±1.9	20.1±3.3
100 sec	0.0028 ±0.00013	0.0019 ±0.00013	0.0006 ±0.00006	37.6±3.3	26.1±1.1	25.1±3.1
150 sec	0.0021 ±0.00038	0.0020 ±0.00050	0.0013 ±0.00063	65.8±24.1	40.6±16.8	38.1±3.5
200 sec	0.0023 ±0.00050	0.0018 ±0.00008	0.0008 ±0.00006	51.8±6.7	36.4±2.5	46.9±6.1

Table 4.3 SDR Model Parameters

Fitting Curve	Loading	Creep	Unloading
Parameters	*E, η, H*	*η*	*E, η*

Note: $E' = \dfrac{E}{(1-v^2)}$

Table 4.4 SDR Model Fitting Parameters

Dwell Time (sec)	Modulus E (GPa)	Hardness H (GPa)	Viscosity (Pa-sec^2)
70	0.34	0.12	5.33E11
100	0.4	0.031	3.92E11
150	0.28	0.008	2.43E11
200	0.295	0.002	2.51E11

Table 4.5 Comparison between nonlinear SDR Model and Oliver-Pharr Model

	Modulus		
Dwell Time (sec)	Nonlinear SDR (GPa)	Oliver-Pharr (GPa)	Comparing SDR to Oliver-Pharr
70	0.34	0.0014	250
100	0.4	0.00023	1500
150	0.28	0.0007	400
200	0.295	0.00055	500

(a) Comparing *E* values from SDR model vs. Oliver-Pharr Model

	Hardness		
Dwell Time (sec)	Nonlinear SDR (GPa)	Oliver-Pharr (GPa)	Comparing SDR to Oliver-Pharr
70	0.12	0.0014	80
100	0.031	0.0002	130
150	0.008	0.00072	10
200	0.002	0.00055	3

(b) Comparing *H* values from SDR model vs. Oliver-Pharr Model

Table 4.6 Comparison between Nonlinear SDR and Linear SDR to Oliver-Pharr Method

Modulus

Dwell Time (sec)	Nonlinear SDR (GPa)	Linear SDR (GPa)	Oliver-Pharr (GPa)	Comparing SDR to Oliver-Pharr	Comparing SDR to Oliver-Pharr
70	0.34	0.372	0.0014	250	265
100	0.4	0.344	0.00023	1500	1500
150	0.28	0.2198	0.0007	400	300
200	0.295	0.16	0.00055	500	300

(a) Comparing *E* values from SDR model vs. Oliver-Pharr Method

Hardness

Dwell Time (sec)	Nonlinear SDR (GPa)	Linear SDR (GPa)	Oliver-Pharr (GPa)	Comparing Nonlinear SDR to Oliver-Pharr	Comparing Linear SDR to Oliver-Pharr
70	0.12	0.114	0.0014	80	80
100	0.031	0.0092	0.0002	130	50
150	0.008	0.08	0.00072	10	110
200	0.002	0.00526	0.00055	3	10

(b) Comparing *H* values from SDR model vs. Oliver-Pharr Method

CHAPTER 5

NANOINDENTATION OF ASPHALT CONCRETE

5.1 INTRODUCTION

Asphalt concrete (AC) consists of coarse aggregate, asphalt binder and fines. The asphalt binder creates an asphalt film around the coarse aggregate and fines. Indeed, fines are trapped inside the binder film, which is also known as mastic. An AC is therefore mastic coated aggregate. Mastic and aggregate governs most of the mechanical properties of AC. Therefore, researchers have performed various tests on mastic to understand macroscale behavior of AC (Huet 1963, Sayegh 1965, Little et al. 1999, Masad et al. 2001, Buttler and You 2001, Guddati et al. 2002, Saad et al. 2004, Xu and Solaimanin 2009, Tarefder et al. 2010, Jager et al. 2010, Zofka et al. 2011). However, nanomechanical characterization is more appropriate for mastic, as the thinness of mastic is about 15 to 20 microns around an aggregate particle. In this study, nanoindentation tests are conducted on mastic and aggregate as an integral part of AC. In particular, modulus and harness of oven aged mastic and aggregate are compared to those of unaged mastic and aggregate.

5.2 METHODOLOGY

5.2.1 Materials

Superpave SP-III mix was collected from a local plant and compacted by a Superpave gyratory compactor in the laboratory.

5.2.2 Aging in AC

The unaged (HMA) specimens were placed in an oven at 85 °C ± 3 °C for 120 ± 0.5 hours. After this time period, the oven was turned off and kept open to allow the specimens to cool at room temperature for 16 hours. The specimens were not disturbed during the cooling period. AASHTO R 30 method is used to simulate long term aging of AC (AASHTO R 30).

5.2.3 Sample Preparation

The HMA mixes were compacted into 15 cm diameter cylinders by a Superpave gyratory compactor using a 600 kPa vertical pressure (AASHTO T 312 2002). Using a water-cooled laboratory saw, a 2.5 cm thick disc was sliced from the center of each cylinder to get samples with uniform air voids. All samples were prepared at a target air void of 4% and polished. A fine laboratory saw at the Geology Department was used to cut and prepare thin AC cubes. A smooth surface is required for nanoindentation tests. The cube surface was polished by a grinding machine with a rotating speed of 150 rpm and a set of SiC paper for decreasing abrasiveness under continuous water cooling. Finally, the samples were washed in a water bath to remove any dust created during the polishing process. Figure 5.1 shows a polished AC sample. The sample surface is marked by an ink pen to show mastic and aggregate.

5.2.4 Nanoindentation Test

A maximum load of 0.28 mN was applied with an unloading rate of 0.01 mN/sec. A creep time of 120 sec was applied after reaching the maximum load. A sitting load of 0.03 mN was used for all the samples. Four AC samples were prepared for

nanoindentation tests. Materials, air voids, compaction procedure and specific gravity remained same for all four samples. Each sample was tested on the mastic portion for 100 indentations. This is to deal with the variability of nanoindentation results due to heterogeneity of asphalt mastic. As an aggregate particle can be expected to have less heterogeneity due to homogeneous or similar mineralogy, only 60 indentations were made on the aggregate portion of each sample.

The nanoindenter device at the University of New Mexico (UNM) laboratory was used for indentation. Figure 5.2 shows the nanoindentation test setup with the Berkovich indenter tip and sample indenting in AC. In nanoindentation test, the AC sample was mounted on a polymer substrate and the sample substrate system held by a sample stub. The pendulum in the system is used to adjust the bridge box output for the Berkovich indenter tip. Figure 5.3 shows the enlarged view of Berkovich tip indenting on the AC surface.

5.3 RESULTS AND DISCUSSION

In the study, nanoindentation tests were done on the aggregate and mastic phase of AC. Figure 5.4(a) shows a schematic aggregate and mastic phase in a square cut sample. In the nanoindentation test on AC, the mastic and aggregate phase of AC was introduced to the indenter tip by visual observation, as the nanopositioner is not available in the nanoindenter at UNM. The complexity of the shared mastic and aggregate system there is a chance that the nanoindenter can hit on the aggregate part that surrounds the mastic. The case will generate the load displacement curve for the aggregate part of the material. To ensure the nanoindenter tip is hitting in the mastic part, 5 by 20 = 10 indentation grid

points were selected. Figure 5.4(b) shows a 500 μm successive distance selected for the grid points. The points covered a 10 mm distance along the row to fit around 130 particles that passed through a #200 sieve. It was possible to select a length more than 10 mm in the sample as mastic phase for nanoindentation. In addition, the average binder thickness on an aggregate phase is 10-15 μm, whereas the maximum indentation depth on the mastic phase is 3μm, as shown in Fig. 5.4(c). Therefore, the thickness difference also confirms that the nanoindenter tip is extracting the load displacement curve for the mastic phase of AC.

Figure 5.5 shows load displacement curves for unaged mastic and aggregate phases of AC. From the figure, it is evident the maximum displacement in the mastic phase is fixed around 3200 nm (Fig. 5.5(a)). However, the maximum displacements of the aggregate phase are found at 400 nm. In addition, the unloading displacement in the mastic phase is found after 400 nm. Thus, the figure clearly illustrates the nanoindenter is not hitting the aggregate parts of the AC. A similar scenario was found for nanoindentation load displacement behavior of an aged AC sample, as shown in Fig. 5.5(b). Fig. 5.6(a) shows the maximum displacement of aged aggregate is 800 nm, whereas from Fig. 5.6(b), the maximum displacement in the mastic part is 2000 nm. Therefore, nanoindentation tests on aged AC extracted the nanoscale load displacement behavior of both aggregate and mastic phases.

The comparative study of load displacement behavior of unaged and aged AC unveils nanoscale behavior due to aging. Comparison of Fig. 5.5(b) and Fig. 5.6(b) shows higher displacement in the unaged mastic phase of AC than the aged mastic phase. The highest displacement found in the unaged mastic for the same load is around 3000 nm, as shown

in Fig. 5.5(b), whereas for aged mastic the highest displacement is around 2000 nm, as shown in Fig. 5.6(b). Therefore, the aging of the sample hardens in the mastic part of the AC, which resembles the age hardening behavior of asphalt.

In nanoindentation tests on AC, a dwell time of 120 sec is applied for all the indentation tests to minimize the viscous effect of the mastic part of AC. However, nose effects were found for some of the load displacement curves of unaged AC. The nose effects of the unloading load displacement curves made it impossible to analyze with Oliver Pharr analysis. The load displacement curves for negatively sloped unloading curves are shown in Fig. 5.7.

The nanomechanical behavior of aggregate is not the same for all indentation points. The creep displacement irregularities as well as the loading curves are showing the nanoscale heterogeneity in the aggregate. The microstructural difference and orientation could be a reason for this anomaly. However, for all the aggregates the load displacement curves have not behaved like an elastoplastic material. The unloading portion of the load displacement curves shows plastic flow instead of regaining its elastic portion of indentation depth (Fig. 5.8). The load displacement curves show that instead of recovering elastic depth, the indentation depth continues to increase. The load displacement behavior is repeated after aging of the sample and tests were completed on the same selected sample.

Figure 5.9 shows pop-in phenomena in the load displacement curve for the AC mastic phase. Pop-in is an obvious finding for the mastic part of AC because of the presence of

air voids in AC. Pop-in is also found in aggregate during nanoindentation (Fig. 5.10). A mineral defect can be the cause for pop-in phenomena in the aggregate part of AC.

During nanoindentation in the AC, the applied dwell time for the nanoindentation tests in the thin material is high enough to decrease the viscous effect to a minimal level. As the viscous effect is in the minimal level with such test setup, it is possible to analyze the unloading curve of load displacement through Oliver Pharr analysis. In Oliver Pharr analysis, the load displacement data is analyzed to determine the elastic modulus and the hardness of the material. The analysis is done on all the indentation curves on unaged and aged load displacement data. Figure 5.11 shows the comparative column charts of elastic modulus and hardness for the mastic part of AC. The average elastic modulus value found in the mastic phase ranges from 0.3 GPa to 6.0 GPa and the average hardness value ranges from 0.1 GPa to 1.5 GPa.

Figure 5.11(a) shows the comparative study of unaged and aged mastic for elastic modulus value. The chart shows that the aged mastic phase of AC loses the elastic property of the material. The loss of the volatile material component of the asphalt material is the cause of age hardening of asphalt. For all the samples in Fig. 5.11(a), the loss of elastic modulus is evident. Each column in the figure represents an average of 100 nanoindentation points. However, sample 3 and sample 4 show higher modulus reduction compared to sample 1 and 2. Nanoindentation tests successfully captured the age hardening behavior of AC. Figure 5.11(b) shows the hardness of AC mastic. The aging process of the material increased the hardness of the mastic. All four samples showed increase in hardness. Aged sample 1, 2 and 3 showed increase in hardness compared to unaged samples as in column charts. However, the hardness value for sample 4 is low

enough that the comparison is not evident from the charts. Aged sample 4 also showed higher hardness value compared to unaged sample. Increase of viscosity is responsible for age hardening in asphalt mastic.

The comparative results of the elastic modulus and hardness on unaged and aged aggregate are shown in Fig. 5.12. For aggregate, the average elastic modulus found is between 6.5 GPa to 30.0 GPa and the hardness in between 1.0 GPa to 7.0 GPa. Figure 5.12(a) shows a comparison of the elastic modulus of aggregate in AC. According to the figure, the aggregates' elastic modulus remained almost the same for both unaged and aged AC. In the figure comparison made between 3 samples only, as one sample aggregate showed plastic flow in unloading load-displacement curve, made impossible to analyze through Oliver-Pharr method. Elastic modulus of sample 1, 2 and 3 remained constant before and after aging in AC. Therefore, the oven aging process did not affect the elastic property of the aggregate. However, the situation is not similar for hardness value of aggregate. Aged sample 1 and sample 2 showed decreases in contact hardness compared to unaged samples, whereas hardness value increased for aged sample compared unaged one. As the nanoindentation tests were not done on the same nanoscale position for unaged and aged aggregate, there can be some differences in hardness for unaged and aged aggregate.

5.4 CONCLUSIONS

In the study, the AC is subjected to nanoindentation to extract the mechanical properties of the mastic phase and the aggregate phase of AC. Nanoindentation tests are done in the

AC with higher creep time, so that the load displacement curve can be analyzed through Oliver Pharr analysis. The conclusions of the study are:

- Successful nanoindentation tests are conducted in the mastic phase and the aggregate phase of AC. Nanoindentation tests can capture the nanomechanical property for both phases as an integral part of AC. The comparative study of load displacement behavior of both the mastic phase and the aggregate phase unveils that nanoindentation testing can capture the material behavior of AC.

- The comparative study of load displacement behavior of nanoindentation tests on the unaged and aged mastic phase of AC shows that the unaged mastic's displacement is lower than that of aged mastic. Therefore, aging of AC hardens the mastic phase of AC.

- The comparative study of the elastic modulus and hardness on mastic shows that the elastic modulus decreases with the aging process and the hardness increases with the aging of the material. The increase of hardness and decrease of elastic modulus resembles the age hardening behavior of asphalt binder.

- In the case of the aggregate, the elastic modulus almost remained the same with oven aging of the AC sample.
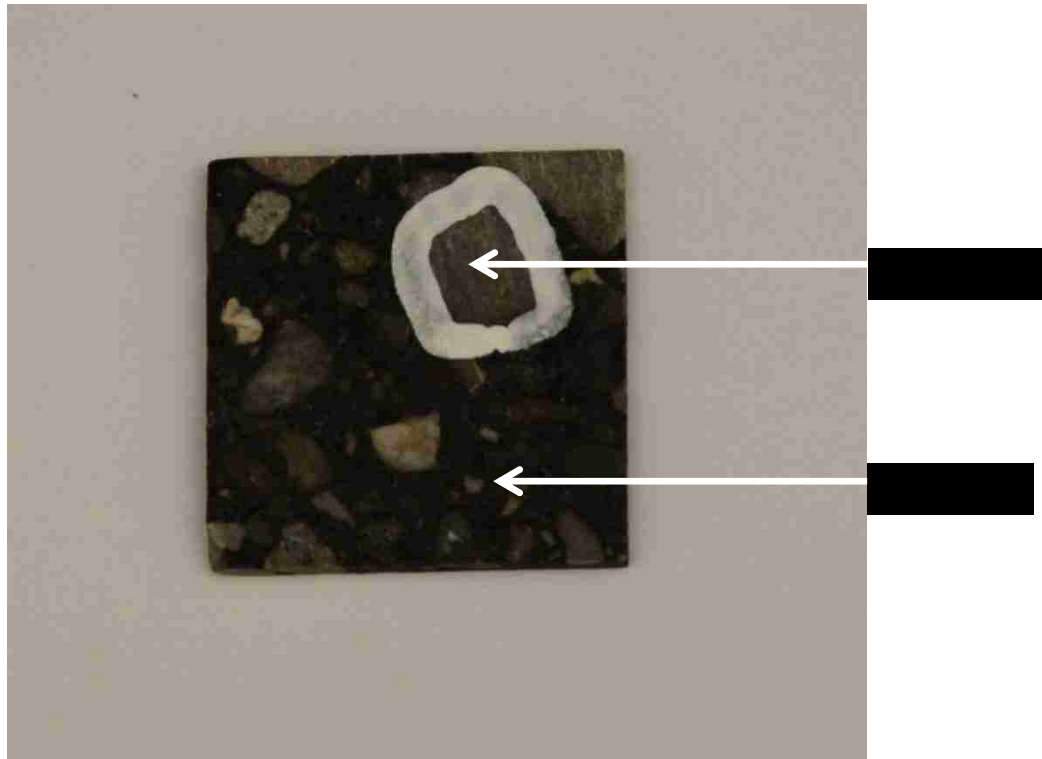
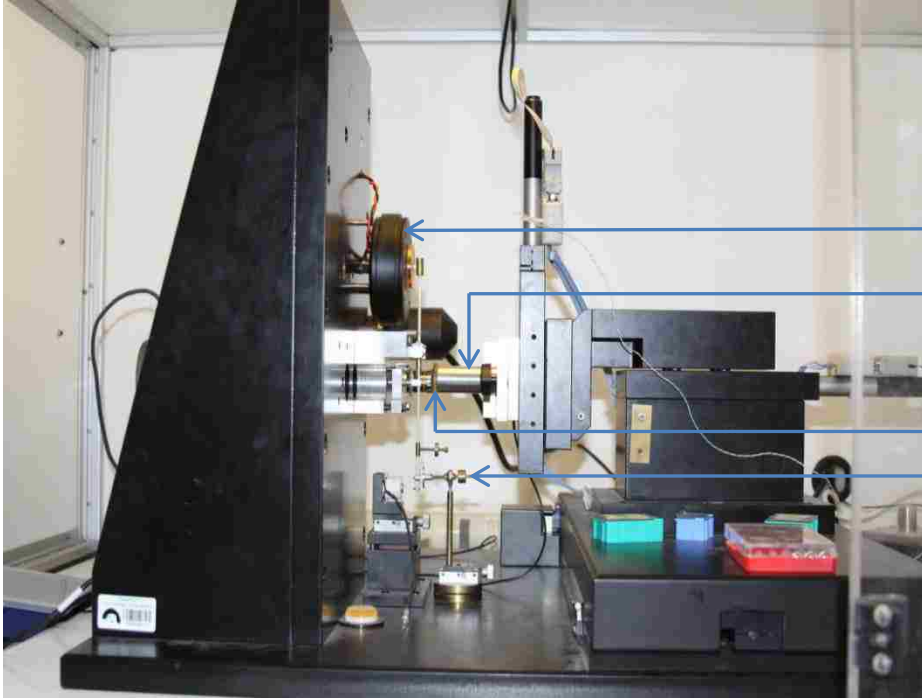**Figure 5.1** Asphalt Concrete (AC) Sample for Nanoindentation

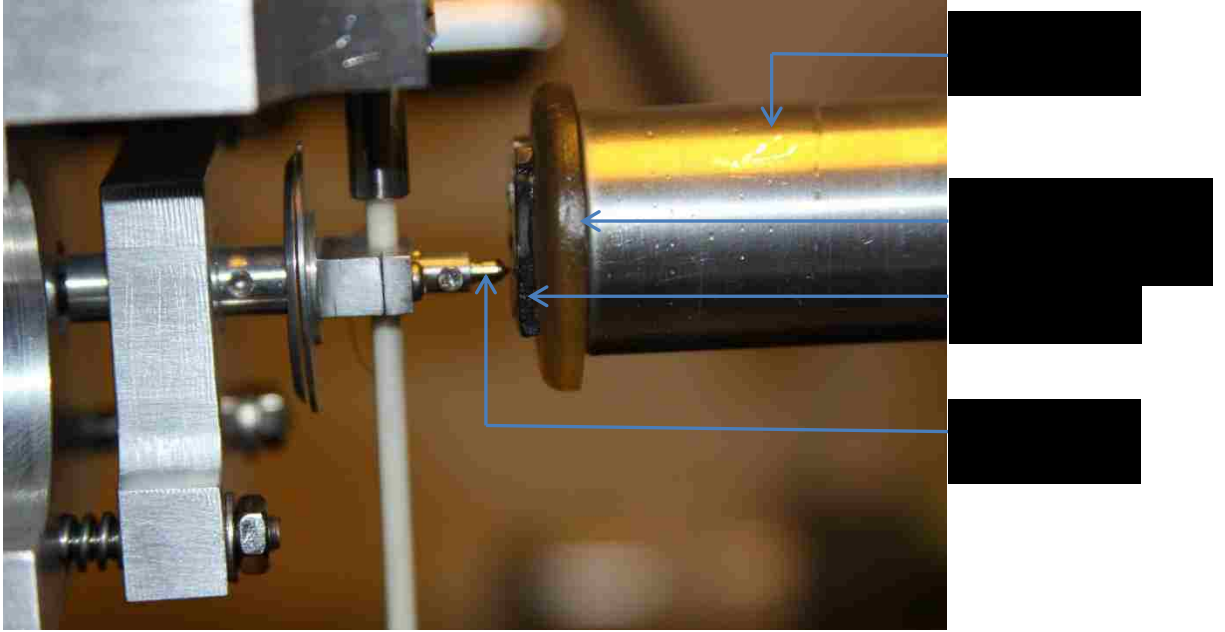**Figure 5.2** Nanoindentation Test Setup for Asphalt Concrete (AC)

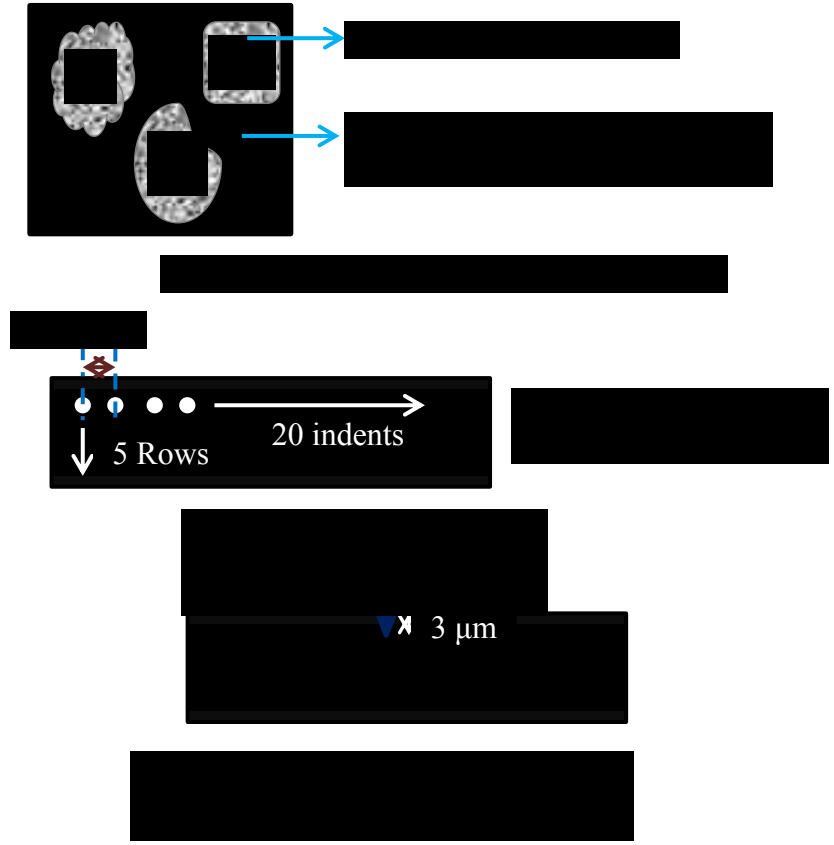**Figure 5.3** Berkovich Tip Indenting on an Asphalt Concrete (AC) Sample
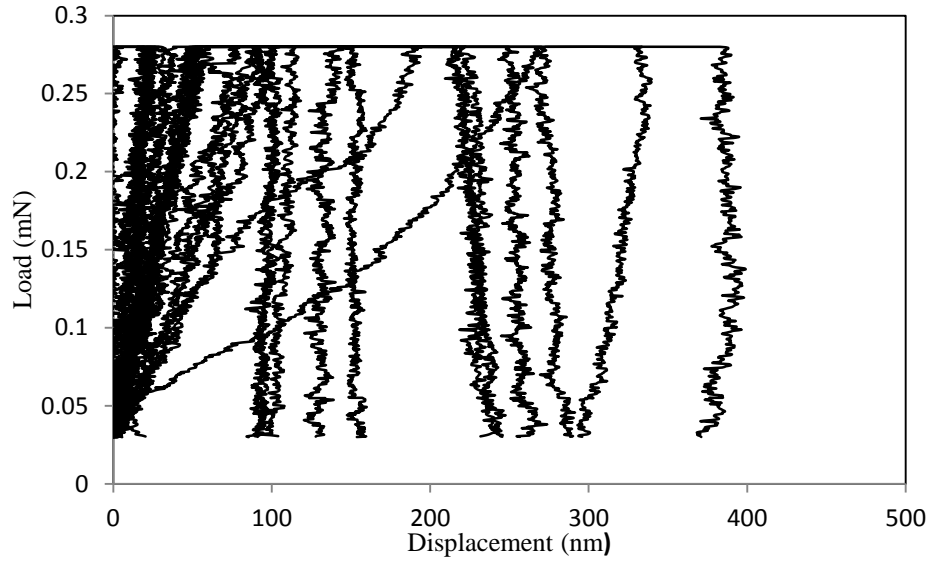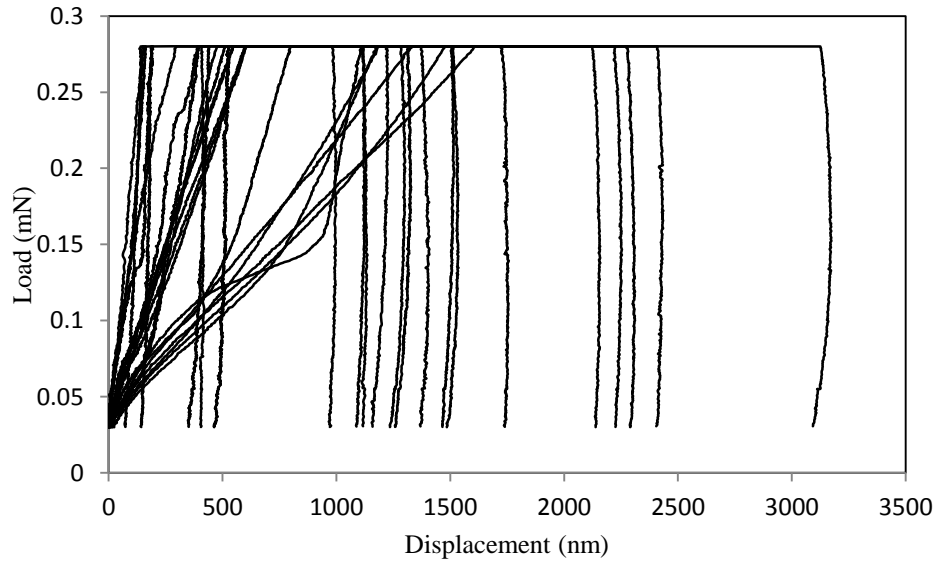
20 indents

5 Rows

3 μm

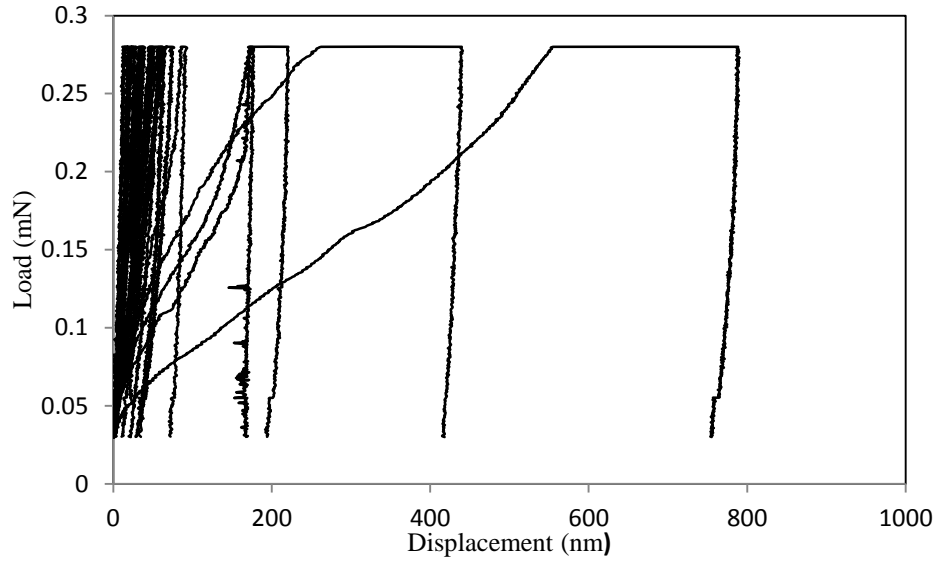**Figure 5.4** Nanoindentation of AC
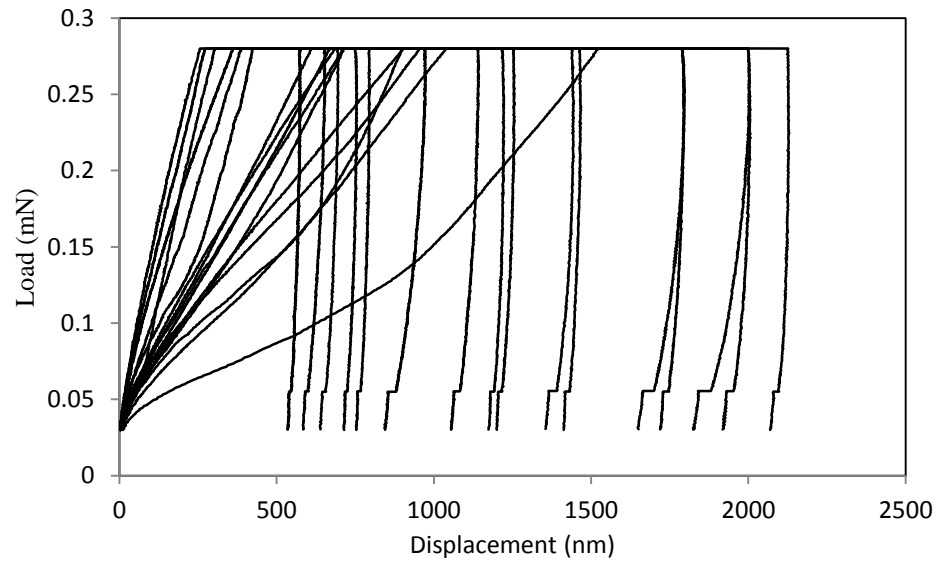
(a) Aggregate Phase

(b) Mastic Phase

Figure 5.5 Load Displacement Curves for Unaged AC

(a) Aggregate Phase

(b) Mastic Phase

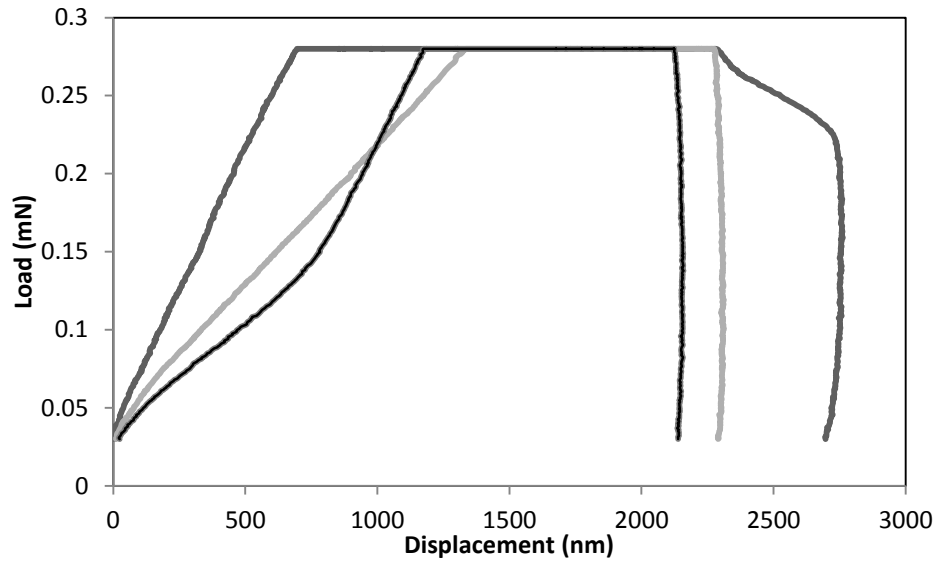**Figure 5.6** Load Displacement Curves for AC

93

Figure 5.7 Negatively Slopped Unloading Curve of Nanoindentation Load Displacement
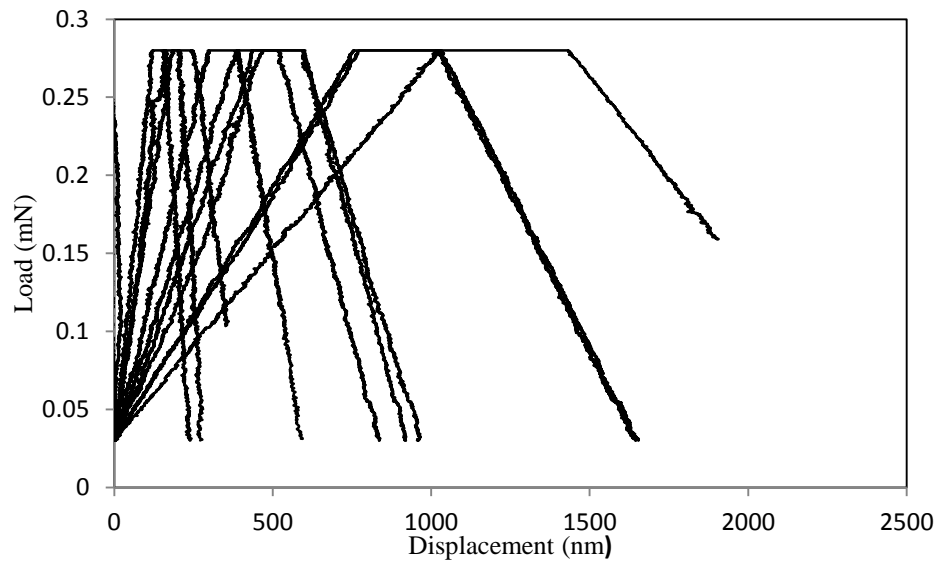
Curve

Figure 5.8 Plastic Flow of Aggregate
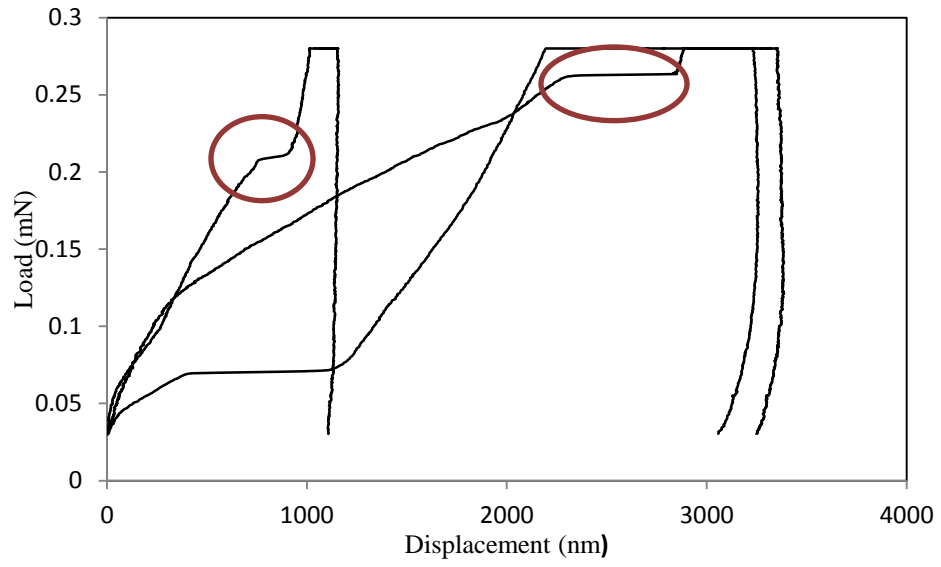
Figure 5.9 Pop-in During Nanoindentation in the Mastic Part of AC
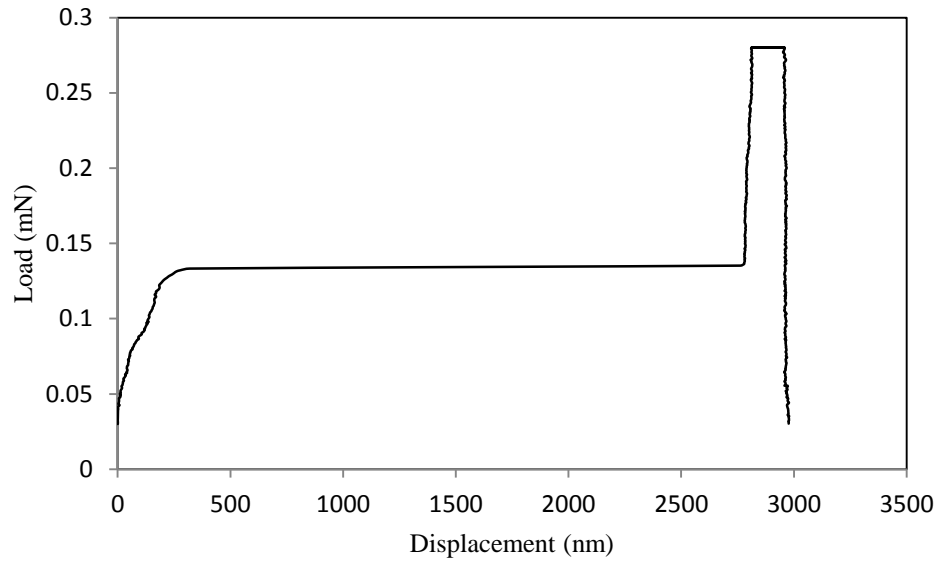
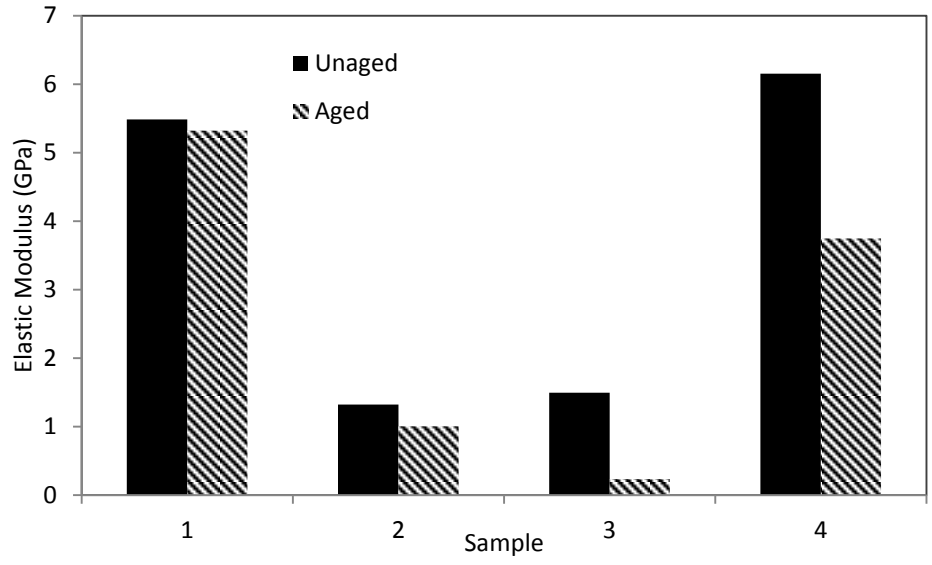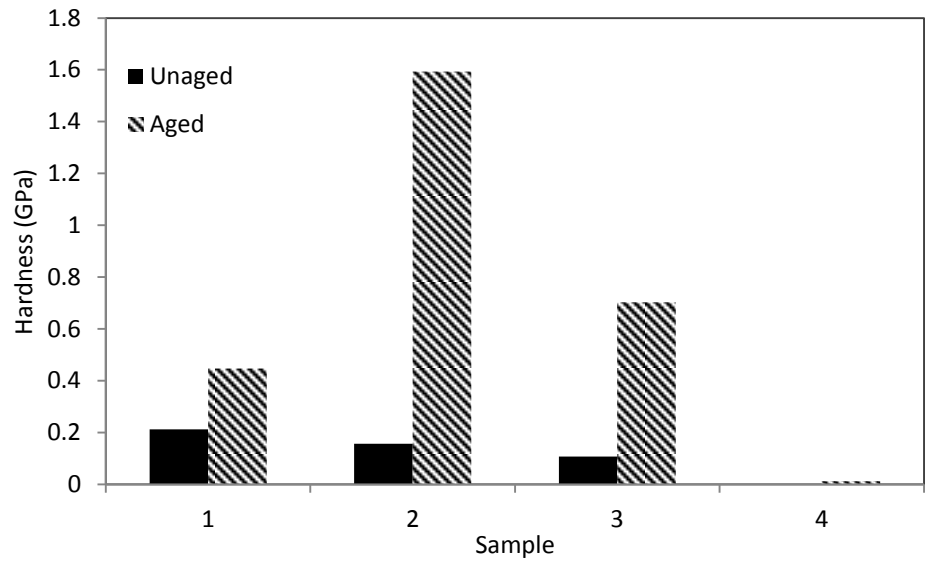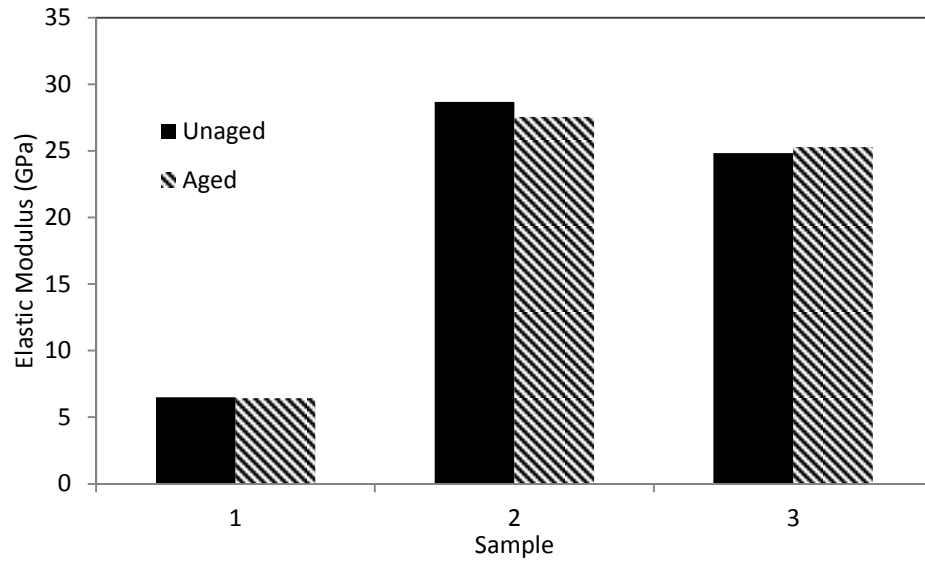**Figure 5.10** Pop-in During Nanoindentation in the Aggregate Part of AC
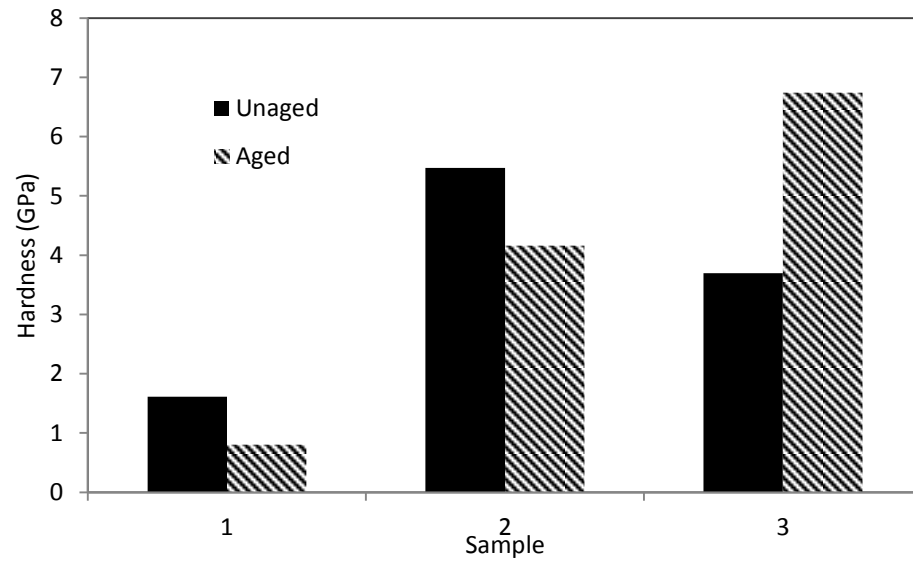
(a) Elastic Modulus

(b) Hardness

Figure 5.11 Nanomechanical Property of Aged and Unaged Mastic Phase of AC

(a) Elastic Modulus

(b) Hardness

Figure 5.12 Nanomechanical Property of Aged and Unaged Aggregate Phase of AC

CHAPTER 6

CONCLUSIONS & RECOMMENDATIONS

6.1 SUMMARY

This study attempts to determine an appropriate model for asphalt and to characterize the nanomechanical properties of asphalt. The nanomechanical characterization is performed by nanoindentation tests on thin film asphalt binders, mastic and aggregate phases of an asphalt concrete. Asphalt being a viscoelastic material the unloading curve of a nanoindentation test is found to have negative slope, which means unloading is affected by the viscosity of asphalt. To that end, two attempts are made in this study. One is to find how nanoindentation modulus and hardness are affected by loading rate and dwell time. Second is to determine modulus, hardness and retardation time from the creep data (not unloading) using rheological and mechanical model consists of dashpot, spring and rigid elements. In addition to testing binders, the mastic and aggregate phases of an asphalt concrete are also tested under nanoindentation.

Traditionally Oliver-Pharr method to analyze indentation data requires a positive slope of the unloading curve. In order to apply Oliver-Pharr analysis, a dwell time is introduced in the study to conduct nanoindentation tests. Berkovich pyramidal indenter tip is used for nanoindentation tests on unaged and aged asphalt binders. However, attempts of indentation on unaged binders failed. The softness of the unaged binder made the nanoindenter tip impossible to detect the contact surface. Nanoindentation tests were conducted successfully on aged asphalt binders. Different combination of dwell time and loading rates were considered in this study. A dwell time greater than 50 sec was able to

produce a positive slope of unloading curve. Specifically, three different loading rates and four different dwell time were used for nanoindentation testing. The loading rates and dwell times were selected so that the indentation depth remained less than 10 percent of the total film thickness to avoid substrate effect on the predicted elastic modulus and hardness of asphalt. The increase in dwell time shows decreased in the predicted elastic modulus and hardness value of asphalt. Higher loading rate, is as expected minimizes the viscous effect of asphalt binder. Increase in dwell time decreases the viscous effect of asphalt binder. Dwell time increase in nanoindentation tests showed decrease in the predicted value of elastic modulus and hardness.

This study attempted to determine E, H and retardation time from creep (dwell time) and loading behavior, instead of unloading curve. This study has employed rheological models such as Voigt model, Burger model and Spring-Dashpot-Rigid (SDR) model to separate the viscous and elastic response of asphalt binder from entire load-displacement curve to avoid dependency on unloading curve. The creep data was also fitted to Burger model. It is shown that retardation time depends on loading rate and dwell time. The viscoelastoplastic model, which is termed as spring-dashpot-rigid (SDR) model in this study, was fitted to the entire load-displacement data of a nanoindentation test on asphalt. The model produced the indentation viscosity, elastic modulus and hardness of the material. The SDR model predicted modulus and hardness values are shown to be higher than those predicted by Oliver Pharr method. In addition, an SDR model with a linear spring element, instead of quadratic spring element, was also tried to fit to indentation data. A poor correlation was found between predicted and laboratory data in case of linear spring.

In this study, nanoindentation tests were also conducted on mastic and aggregate phases of asphalt concrete (AC) to extract the nanomechanical properties as an integral part of AC. While binder is an important constituent of an AC, mastic has been reported by previous studies as equally important (Buttler and You 2001, Tarefeder et. al. 2010). Mastic phase of AC is defined by an asphalt film entrapping fines that pass through #200 sieve. Indentation was performed at numerous grid points of mastic sample to capture the heterogeneity in the mastic phase of AC. It can be noted that nanoindentation test successfully captured the nanoindentation load displacement behavior of mastic phase and aggregate phase of AC. Tests on these two phases include unaged and aged AC samples. AASHTO R 30 was used to simulate long term aging in AC. The average elastic modulus value found in the mastic phase ranges from 0.3 GPa to 6.0 GPa and the average hardness value ranges from 0.1 GPa to 1.5 GPa. For aggregate, the average elastic modulus found is between 6.5 GPa to 30.0 GPa and the hardness in between 1.0 GPa to 7.0 GPa.

6.2 CONCLUSIONS

Based on the findings of this study, the following conclusions:

- Limited attempts were made to indent an unaged asphalt sample, which are soft. Nanoindentation tests on unaged asphalt binders failed because the indenter tip was unable to detect and establish the contact surface. It is essential that a tip establish a contact surface before proceed.

- Based on the Oliver-Pharr prediction of elastic modulus and hardness, it is shown that as the dwell time increases the value of both apparent elastic modulus and

hardness decrease. The apparent elastic modulus and hardness values decrease as the loading rate increase in a nanoindentation test.

- At a small dwell time (less than 50 sec) and low loading rate (less than 0.002 mN/sec) the unloading portion of the load displacement curve shows a bowing out or nose effect. To make the load displacement data to be analyzed by traditional Oliver Pharr analysis a dwell time of greater than 50 sec and loading rate of greater than 0.007mN/sec are recommended for conducting nanoindentation test on asphalt binder.

- Rheological models such as Voigt model and Burger model are employed to determine the viscoelastic behavior of an asphalt binder. Results show that the retardation time increases as loading rate and dwell time increase in nanoindentation tests on asphalt. It is also noted that the predicted model parameters can determine the creep compliance and viscosity of asphalt binder.

- A SDR model was fitted to the load-displacement behavior of nanoindentation on asphalt binder. Apparent modulus and hardness decrease with an increase in dwell time. In addition, a SDR model with linear response of spring shown not to have a good fit to indentation data.

- Nanoindentation tests were successfully conducted on mastic phase as well as the aggregate phase of an AC. Aged mastic showed lower elastic modulus and higher hardness value than those of unaged mastic of an AC. The increase of hardness and decrease of elastic modulus resembles the age hardening behavior of asphalt binder. Aged aggregate material's E and H remained same.

6.3 RECOMMENDATIONS

The following points can be recommended for future studies:

- Development of new test procedure for nanoindentation on unaged asphalt binder using the indentation impression on unaged asphalt binder sample.

- Effects of maximum load and test temperature on asphalt binders' E, H and retardation time were not investigated in this study.

- Degree of Aging affects E and H but it is not known yet how and by what amount. Degree of aging can be studied in future.

REFERENCES

ASTM Standard E2546 – 07. "Standard Practice for Instrumented Indentation Testing." ASTM International, West Conshohocken, PA, DOI: 10.1520/E2546-07, www.astm.org.

Bembey, A. K., Oyen, M. L., Bushby, A. J., and Boyde, A. (2006). "Viscoelastic properties of bone as a function of hydration state determined by nanoindentation." *Philosophical Magazine*, 86(33–35) SPEC. ISSUE, 5691–5703.

Briscoe, B. J. , and Ozkan, N. (1998). "Characterization of ceramic pastes by an indentation hardness test." *J. of the European Ceramic Society*, 17(14), 1675–1683.

Briscoe, B. J., and Sebastian, K. S. (1996). "Elastoplastic response of poly(methyl methacarylate) to indentation." *Proc. of the Royal Society of London*. 452(1946), 439–457.

Cheng, Y., and Cheng, C. (1998). "Can stress-strain relationships be obtained from indentation curves using conical and pyramidal indenters?" *J. of Mater. Res.*, 14(9), 3493–3496.

Doerner, M. F., and Nix, W. D. (1986). "A Method for interpreting the data from depth-sensing indentation instruments." *J. Mater. Res.*, 1(4), 601–609.

Feng, G., Ngan, A.H.W (2002). "Effects of creep and thermal drift on modulus measurement using depth-sensing indentation." Journal of Materials Research, 17(3), p 660-668.

Fischer-Cripp, A. (2004). "Nanoindentation." *Mechanical engineering series*, 2nd Ed., Springer, New York.

Huang, G., Lu, H. (2006). "Measurement of Young's relaxation modulus using nanoindentation." *Mechanics of Time-Dependent Materials*, 10(3), 229-243.

Isaksson, H., Nagao, S., Makiewicz, M., Julkunen, P., Nowak, R., Jurvelin, J. (2010). "Precision of nanoindentation protocols for measurement of viscoelasticity in cortical and trabecular bone." *Journal of Biomechanics*, 43(12), 2410-2417.

Jager, A., Lackner, R., and Sangl K. (2010). "Microscale characterization of bitumen-back analysis of viscoelastic properties by means of nanoindentation." *Int. J. Mater. Res. (formerly Z. Metallkd.)* 98, 404–413.

Kim, Y., Richard (2009), "Modeling of Asphalt Concrete." *ASCE Press*

Lee, C., Lee, S., Sung, L., and Nguyen, T. (2006). "Load-displacement relations for nanoindentation of viscoelastic materials." *J. of App. Physics*, 100(3), 9.

Monclus, M.A., Jennett, N.M. (2011). "In search of validated measurements of the properties of viscoelastic materials by indentation with sharp indenters." *Philosophical Magazine*, 91(7-9), 1308-1328.

Olesiak, S. E., Oyen, M. L. and M. L., Ferguson, V. L. (2009). "Viscous behavior in Berkovich nanoindentation of bone." *Soc. for Experimental Mech. - SEM Annual Conf. and Exposition on Experimental and Applied Mechanics*, 3, 1803–1809.

Oliver, W. C., and Pharr, G. M. (1992). "An improved technique for determining hardness and elastic modulus using load and displacement sensing indentation experiments." *J. Mater. Res.*, 7(6), 1564–1583.

Oyen, M. L., and Cook, R. F. (2002). "Load-displacement behavior during sharp indentation of viscous-elastic-plastic materials," *J. of Mater. Res.*, 18(1), 139-150.

Oyen, M. L., and Ko, C. (2007). "Examination of local variations in viscous, elastic, and plastic indentation responses in healing bone," *J. of Mater. Sci.: Mater. in Medicine*, 18(4), 623–628.

Pharr, G. M., and Bolshakov, A. (2002). "Understanding nanoindentation unloading curves.*" J. of Mater. Res.*, 17(10), 2660–2671.

Tai, K., Qi, H. J., and Ortiz, (2005). "Effect of mineral content on the nanoindentation properties and nanoscale deformation mechanisms of bovine tibial cortical bone." *J. of Mater. Sci.: Mater. in Medicine*, 16(10), 947–959.

Tarefder, R. A., Arifzaman, M. (2010). "Nanoindentation Study on Moisture Damage in Asphalt Concrete." 8th International Transportation Specialty Conference, 1578-1587.

Tarefder, R. A., Zaman, A. M., and Uddin W. (2010). "Determining Hardness and Elastic Modulus of Asphalt by Nanoindentation.*" J. of Geomech.,* 10(3), 106–116.

Wang, J., and Ovaert, T.C., (2008). "Computational mechanical property determination of viscoelastic/plastic material from nanoindentation creep test data." *J. of Mater. Res.*, 24(3), 1245–1257.

Wei, B., Zhang, T., Li, W., Xing, D., Xang, L., and Wang, Y. (2005). "Indentation creep behavior in Ce-based bulk metallic glasses at room temperature." *Mater. Transactions*, 46(12), 2959–2962.

Wu, Z., Baker, T. A., Ovaert, T. C., and Niebur, G. L. (2011). "The effect of holding time on nanoindentation measurements of creep in bone." *J. of Biomech.*, 44(6), 1066–1072.

Yang S., Zhang Y., and Zeng K. (2004). "Analysis of nanoindentation creep for polymeric materials." *J. of Appl. Phy.*, 95(7), 3655–3666.

Yousefi, S. S. (2010). "Rheological and Nanomechanical characterization of aging in polymer modified asphalt." M.S. Thesis, University of New Mexico.

Zhang, H., and Fang, Z. Z. (2008). "Characterization of quasi-plastic deformation of WC-Co composite using Hertzian indentation technique." *Inter. J. of Refractory Metals and Hard Mater.*, 26(2), 106–114.

Zhang, C.Y., Zhang, Y. W., and Zeng, K. Y. (2004), "Extracting the mechanical properties of a viscoelastic polymeric film on a hard elastic substrate." *J. of Mater. Res.*, 19(10), 3053–3061.

Zhang, C. Y., Zhang, Y. W., Zeng, K. Y., and Shen, L. (2005), "Nanoindentation of polymers with a sharp indentation." *J. of Mater. Res.*, 20(6), 1597–1605.

Ziheng, W. , Baker, T. A., Ovaert, T. C., and Niebur, G. L. (2011). "The effect of holding time on nanoindentation measurements of creep in bone." *J. of Biomech.*, 44(6), 1066–1072.

Zofka, A., Nener-Plante, D. (2011). "Determination of Asphalt Binder Creep Compliance Using Depth-Sensing Indentation." *Experimental Mechanics*, 51(8), 1365-1377.